Fakultät für Medizin

Abteilung für diagnostische und interventionelle Neuroradiologie

Non-invasive modulation of brain functional networks

Juan Gabriel Castrillon Guzman

Vollständiger Abdruck der von der Fakultät für Medizin der Technischen Universität München zur Erlangung des akademischen Grades eines

Doctor of Philosophy (Ph.D.)

genehmigten Dissertation.

Vorsitzender: Prof. Dr. Arthur Konnerth

Betreuer: Priv.-Doz. Dr. Valentin Riedl

Prüfer der Dissertation:

1. Priv.-Doz. Dr. Sandro Krieg

2. Priv.-Doz. Dr. Thomas Töllner

Die Dissertation wurde am 13.06.2018 bei der Fakultät für Medizin der Technischen Universität München eingereicht und durch die Fakultät für Medizin am 10.09.2018 angenommen.

Abstract

This thesis covers two consecutive projects which aim to improve our understanding of well-established methods to imaging and manipulate brain activity. In the first project, I established a novel approach to acquire high-resolution functional brain imaging data. In a second project, I systematically tested the different effects of brain stimulation on local and global neural activity in the human brain.

Functional magnetic resonance imaging (fMRI) is currently the most widely applied method to non-invasively study human brain activity. The development of new acceleration methods referred to as multiband (mb), allows us shortening the acquisition times of fMRI by simultaneously acquiring multiple slices. However, these methods have an impact on image quality, which has only been partially investigated up to now. To evaluate this impact, I acquired fMRI datasets using different mb factors. I evaluated the effect of mutiband acceleration on both the image quality and the sensitivity to detect brain network activity. I observed that images obtained using a mb acceleration factor of 2 did not impact on the image quality but increased significantly the sensitivity and stability in detecting brain network activity. In summary, this allows to acquire brain imaging data in half the regular acquisition time.

Non-invasive brain stimulation methods, particularly transcranial magnetic stimulation (TMS), reliably modulate human perception and behavior. However, the influence of TMS on brain activity and communication among sensory and higher cognitive brain systems is still unclear. To estimate this influence, I stimulated brain regions located in a sensory, a high-cognitive, and a control network. For each target node, I then investigated the stimulation effect on the local, network and global brain activity with multiband-accelerated resting state fMRI. I found that TMS has (i) no effects on the local brain activity, (ii) an opposite effect on the network brain activity; and (iii), that TMS increased global brain functional integration of weakly integrated areas such as the sensory and control nodes. To conclude, I suggest that brain functional integration serves as a predictable marker for cortical spreading effects of TMS.

Zusammenfassung

Diese Doktorarbeit umfasst zwei aufeinanderfolgende Projekte, deren Hauptziel es ist, etablierte Methoden zur Bildgebung und Beeinflussung von Gehirnaktivität besser zu verstehen. In dem ersten Projekt entwickelte ich einen neuartigen Ansatz zur Erfassung hochauflösender funktioneller Bildgebungsdaten. In einem zweiten Projekt testete ich systematisch verschiedene Effekte, die eine konventionelle Hirnstimulationsmethode auf lokale und globale Gehirnaktivität hat.

Funktionelle Magnetresonanztomographie (fMRT) ist die am weitesten verbreitete Methode, um die menschliche Gehirnaktivität nicht-invasiv zu untersuchen. Neue Beschleunigungsverfahren, die als Multiband (mb) bezeichnet werden, ermöglichen verkürzte Akquisitionszeiten von fMRT durch die gleichzeitige Aufnahme mehrerer Schichten. Die Auswirkungen dieser Methoden auf die Bildqualität sind jedoch bisher nur begrenzt bekannt. In der vorliegenden Arbeit untersuchte ich deshalb die Auswirkungen mehrerer mb-Faktoren auf die Bildqualität und verglich die Sensibilität zur Detektierung von Netzwerkaktivität im menschlichen Gehirn mit konventioneller fMRT. Ich beobachtete, dass mit einem mb-Beschleunigungsfaktor von 2 die Netzwerkaktivität des Gehirns mit signifikant höherer Sensitivität und Stabilität ermittelt werden kann. Somit lässt sich die Hirnaktivität in der Hälfte der regulären Aufnahmezeit messen.

Nicht-invasive Hirnstimulation, insbesondere die transkranielle Magnetstimulation (TMS), sind verlässliche Verfahren zur gezielten Modulation menschlicher Wahrnehmung. Jedoch ist der Einfluss von TMS auf die Hirnaktivität und die Kommunikation zwischen sensorischen und höher kognitiven Hirnsystemen unklar. Für diese Arbeit stimulierte ich kortikale Regionen in einem sensorischen, einem hoch-kognitiven und einem Kontroll-Netzwerk. Danach untersuchte ich den Stimulationseffekt auf die lokale, Netzwerk- und globale Gehirnaktivität mit Ruhezustand fMRT. Die Ergebnisse zeigen, dass (i) TMS keine Auswirkungen auf die lokale Hirnaktivität hat, (ii) TMS eine entgegengesetzte Wirkung auf die Netzwerkhirnaktivität hat und (iii), dass TMS von schwach integrierten Hirnregionen die funktionelle Integration des gesamten Gehirns erhöht. Die funktionelle Integration des Kortex ist somit ein verlässlicher Indikator zur Beschreibung der TMS-Wirkung auf globale Hirnaktivität.

Acknowledgement

I am very grateful, first, to my family, especially my mother and sisters, for all their life-long unconditional love and support. Second, to my supervisor Valentin for his support and inspiring guidance who encouraged me not only to be engaged with the project but also to enjoy every day more what I do. Third, to Norita for her love and positives vibes, cheering me up during the stressful times of the thesis writing.

Fourth, to all the people and Institutions who supported me during the studies. Colciencias in Colombia for funding my studies. Prof. Zimmer and the Department of Neuroradiology of the TUM for providing all the facilities necessaries to develop this project. The Instituto de Alta Tecnologia Medica in Colombia of their unconditional support. The members of my TAC committee for their constructive feedback, especially to Sandro Krieg for his support with the TMS project. Christine Preibisch for her support with the optimization of the MRI sequences. Kasia and Nico for their help during the long and marathon data acquisition sessions.

Finally, to every one of the wonderful human beings in my life who fuel my spirit with happiness, Miguel and our entertaining conversations while having a nice beer or coffee; Nichu, my greek sister; Kasia and our working days full of joy; Judita and our active pauses; my beloved Aurora, Martina, Deniz and Georgiana; my office mates Lollo, Lukas, Tim, Monica and Isabel; the Locombians in München Hans, Alex, Gina, Eliana and Juliana; my Bavarian family Brigitte, Ludwig and Denis; Sebastian, with whom I started the adventure in München; Raul, Siri, Adriana, Camilo, Jaime, Luis, Paola, Catalina and all the friends from an interminable list who have shaped who I am today.

Contents

1 Introduction

The relationship between human brain signaling and behavior is a central concern of neurosciences. Hitherto, it has been mostly studied using neuroimaging techniques, which correlate different aspects of the brain structure and function with a behavioral test associated with an underlying cognitive function. However, this purely correlative approach allows no causal conclusions to be derived. Hence, brain stimulation methods have been used to directly induce changes in neural processes that affect behavior and the underlying cognitive function of interest. These include pharmacological interventions, targeted microstimulation, or optogenetics. Such methods allow us to derive brain–function relationships with high spatial and temporal resolution, even at the cellular level. Nevertheless, they are usually invasive, and consequently, generally inadmissible for use in studies on human subjects. The study of causal relationships between brain and behavior employing non-invasive brain stimulation techniques (NIBS) allows us to derive causal relationships between brain anatomy and function with behavior in patients or healthy subjects.

The most popular NIBS technologies are electromagnetic, using either electrical stimulation or magnetic fields: transcranial electrical stimulation (tES) and transcranial magnetic stimulation (TMS). Both methods can causally manipulate neural activity at a mesoscale spatial level (cortical tissue, gyri) and their temporal effect is between a couple of seconds to minutes, depending on the type of stimulation (Fig. 1.1). Moreover, it has been shown that the NIBS methods can induce changes beyond the stimulated region. Where this is the case, the spatial extent of the stimulation effects should be interpreted carefully, and, whenever possible, should be assessed using neuroimaging. The selection of the neuroimaging technique depends on the research question to be addressed and the specific considerations of the study. However, functional magnetic resonance imaging (fMRI) is the most commonly used due to its high spatial resolution and the possibility of mapping neuromodulatory effects, such as those triggered by arousal, attention, memory, etc., which are slow and can be mapped with this technique [Logothetis, 2008] and to measure the extension of the TMS effect and how the connected brain networks are affected by the application of the stimulation [Polania et al., 2018].

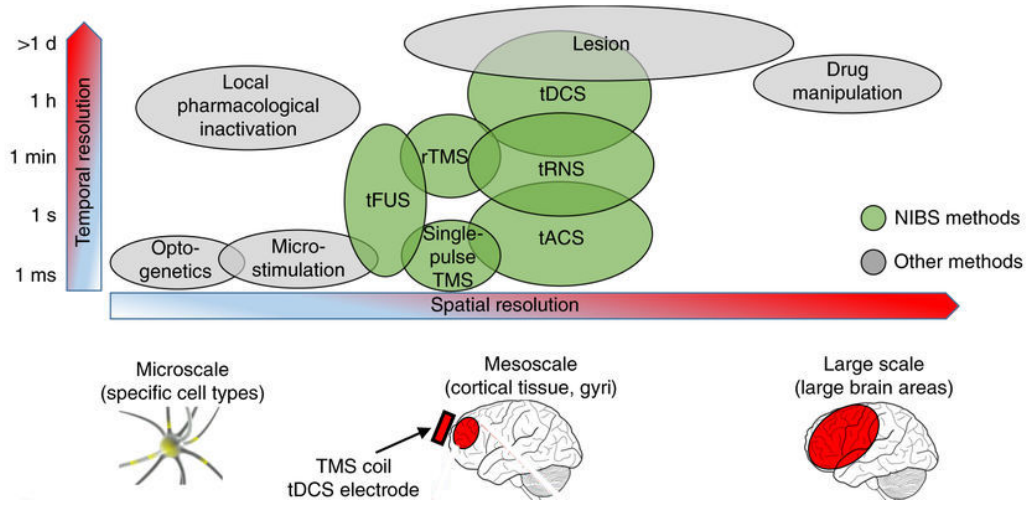

Fig. 1.1: The temporal and spatial resolution of NIBS methods. NIBS methods work at the middle spatial resolution level (mesoscale), with a variable temporal resolution depending on the specific method. Image licensed under creative commons and taken from Polania et al. [2018]

1.1 Transcranial magnetic stimulation

Transcranial Magnetic Stimulation (TMS) is a NIBS method that stimulates cortical areas of the brain by positioning a magnetic field generating coil to the head of the participant. Via electromagnetic induction small electric currents alter neuronal activity in the brain region just under the coil [*OHBA-Oxford*]. The type and duration of the stimulation effect depend on the parameters used (Section 1.1.2)), influencing the induced physiological and behavioral effects on the brain function, and thus, the experimental design when combined with a neuroimaging method. Moreover, the anatomical and functional MR images of each participant can be used to guide TMS target area selection, using the neuronavigation system available in almost all new TMS systems (Fig. 1.2).

1.1.1 Neurophysiological effect

Based on the magnetic induction principle, a rapidly changing high intensity electrical current is passed through a loop of conducting wire inside the TMS coil, generating a magnetic field that penetrates the scalp and is able to induce an electric current in the cortical areas of the brain. The induced currents depolarize the membrane potentials in the surrounding cortical tissue under the coil, opening voltage sensitive ion channels and actively initializing action potentials [Reithler et al., 2011; Valero-Cabré et al., 2017]. The direction of the induced current is perpendicular to the coil surface and its intensity is proportional to the distance from the coil.

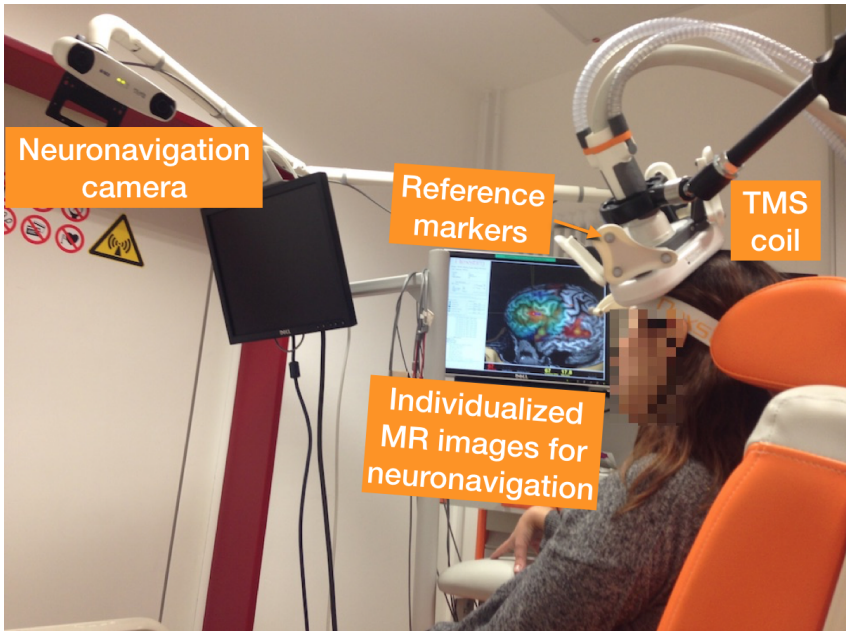

Fig. 1.2: Neuronavigated TMS equipment. The TMS coil is placed tangentially to the head, over the area of interest, which is located with the assistance of the neuronavigation system, an optical navigation tracking technology which shows in real-time the location of the coil. The tracking is based on the registration between the participant MRI images and the reference markers located around the coil and on the head of the participant, which are tracked by the infrared camera.

When it is applied to sensory-motor areas, it can induce a visible response, like a muscle contraction when a motor area is stimulated, or sparking lights, so-called phosphenes, when a visual area is stimulated (Fig. 1.3).

On the other hand, when it is applied to cortical areas associated to high-cognitive functions, such as language, memory, attention, etc., TMS induces no body response such as muscle contractions nor phosphenes, but it interferes with normal cognitive processing and alters communication between interconnected regions and the stimulated one [Valero-Cabré et al., 2017]. The TMS effect depends on several factors, such as the magnetic coil, the stimulation intensity, frequency, duration, and location of stimulation. All these factors influence the type, duration, and efficacy of the neural modulation.

1.1.2 TMS parameters

- **Shape of the magnetic coil**: This determines the magnitude and spatial extent of cortical stimulation. Round coils are relatively powerful, being the figure-of-eight shaped coils most commonly used in TMS studies. This coil produces a focal electrical current at the intersection of the two round components

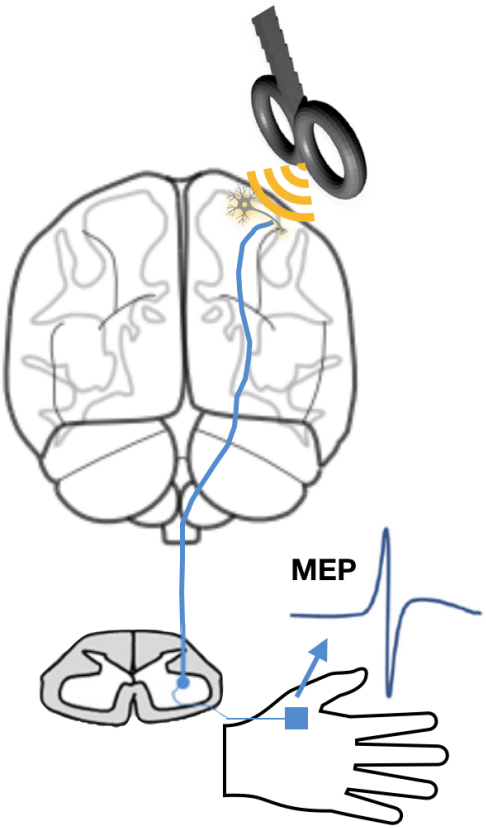

Fig. 1.3: Representation of the neurophysiological effect of TMS. First, the stimulation depolarizes the neurons of the cortical target area. Then, an action potential is induced. This action potential is transmitted synaptically onto the corticospinal neurons and the spinal cord, reaching the muscle and generating a motor evoked potential (MEP) [Bestmann and Feredoes, 2013].

[Hallett, 2007]. In order to minimize the coil-cortex distance, the coil should be placed tangentially to the skull [Hartwigsen et al., 2009].

- **Number of pulses**: While a single TMS pulse disrupts the cortical tissue under the coil for a short period of time, repeated pulses are commonly used to induce long-lasting effects [Fox et al., 2012]. Repetitive TMS (rTMS) refers to the application of prolonged trains of stimuli, which are either given continuously as long trains at a constant rate or intermittently as repetitive bursts.

- **Frequency**: This conditions the effect of the intervention. While trains of low frequency and continuous stimulation (between 300 and 900 pulses) tend to inhibit or suppress the excitability of cortical target areas (inhibitory TMS), high frequency, and discontinuous stimulation tend to excite or increase the excitability of cortical target areas (excitatory TMS) [Valero-Cabré et al., 2017].

- **Intensity**: This is participant-dependent and needs to be adjusted to a level that induces currents in the neural tissue. In motor and visual cortical areas it is set by adjusting TMS intensity to a level inducing visible muscle activation

or a subjective report of phosphene perception [Valero-Cabré et al., 2017]. For other types of cortical areas, the motor threshold is usually used, which is calculated by stimulating the primary motor cortex (M1) and detecting the lowest intensity required to produce a brief muscle contraction in the contralateral hand. It is referred to as the resting motor threshold (rMT) or active motor threshold (aMT) depending on whether the participant hand muscle was relaxed or contracted at the time point of determination [Reithler et al., 2011].

- **Duration**: when TMS is applied in long patterns of individual pulses, cortical activity remains altered for an average period of 30 min post-stimulation for rTMS [Huber et al., 2007; Thut and Pascual-Leone, 2009; Werf and Paus, 2006; Valero-Cabré et al., 2017], or it can have up to 60 min post-stimulation effect for repetitive bursts stimulation [Schindler et al., 2008; Valero-Cabré et al., 2017].

1.1.3 TMS modalities

Different TMS protocols may be generated according to the number of pulses and their duration, the time between pulses or pulse-trains, and the inter-burst discharge frequency [Valero-Cabré et al., 2017]. Together, these parameters define two main modes of stimulation, repetitive and theta-burst TMS.

Repetitive TMS (rTMS)

This refers to the delivery of multiple repetitions of TMS at a particular frequency, which at slow rates (0.2 - 1 Hz) will cause a decrease in brain excitability [Chen et al., 1997], whereas at faster rates (>5 Hz) will cause an increase in brain excitability [Pascual-Leone et al., 1994; Hallett, 2007].

Theta-burst stimulation (TBS)

This is a type of rTMS, where trains of short and fast rTMS stimuli are delivered at the theta frequency ($\sim$5 Hz). The most common paradigm is a train of three stimuli at 50 Hz, repeated at 5 Hz. If given intermittently, for example 2 s of stimulation every 10 s, it is called intermittent TBS (iTBS) and it leads to increased excitability. If it is given continuously over 40 s, it is called continuous TBS (cTBS) and it leads to decreased excitability [Hallett, 2007].

1.1.4 Measuring the TMS effect

When applied to motor or visual areas, TMS can elucidate a detectable behavioral response (Section 1.1.2). Nonetheless, for cortical regions other than sensory-motor areas, where no physiological response outside the brain can be observed, the TMS effect might be assessed by neurophysiological parameters close to the stimulation site [Reithler et al., 2011]. Moreover, evidence suggests that TMS modulates neuronal activity far beyond the site of stimulation, having a distributed effect on brain function. Hence, its effects have been usually assessed using neuroimaging, which allows us to observe the temporal and spatial extent of brain stimulation.

Given the variety of different neuroimaging methods, selection depends on the research question to be solved and the specific considerations of the study. While electroencephalography (EEG) or magnetoencephalography (MEG) are able to map the neural electrical activity changes derived from stimulation with a high temporal resolution, positron emission tomography (PET) or functional magnetic resonance imaging (fMRI) map the glucose metabolism or cerebral blood flow changes derived from stimulation with a high spatial resolution. Each of these methods offer unique advantages and disadvantages, starting with the trade off between temporal and spatial resolution, or the use of radionuclides for mapping the glucose metabolism. Here, I mapped the TMS effect with fMRI due to *(i)* its whole brain coverage with relatively high spatial resolution, allowing me to evaluate its remote effects, *(ii)* its feasibility for within-subject design, minimizing the inter-subject variability which has been reported to be high for stimulation effects [Valero-Cabré et al., 2017; Polania et al., 2018], and *(iii)* the possibility of conducting task-free studies, in order to prevent TMS effects not being captured by a specific behavioral task or paradigm [Fox et al., 2012].

1.2 Functional magnetic resonance imaging

1.2.1 Physics of MRI

Magnetic resonance imaging (MRI) is an imaging technique that detects magnetic moments of nuclei using their orientation in a strong magnetic field and their response at a specific resonance frequency. All elementary particles (electron, proton, neutron, etc.) have a magnetic momentum or 'spin', which can be described as the quantity of rotation of the particle spinning around an axis. In a sample, the nuclear magnetization is the sum of the individual magnetic moments per unit volume. In the presence of an external magnetic field, the atoms rotate around the direction of an external magnetic field at a characteristic frequency of each nucleus, which

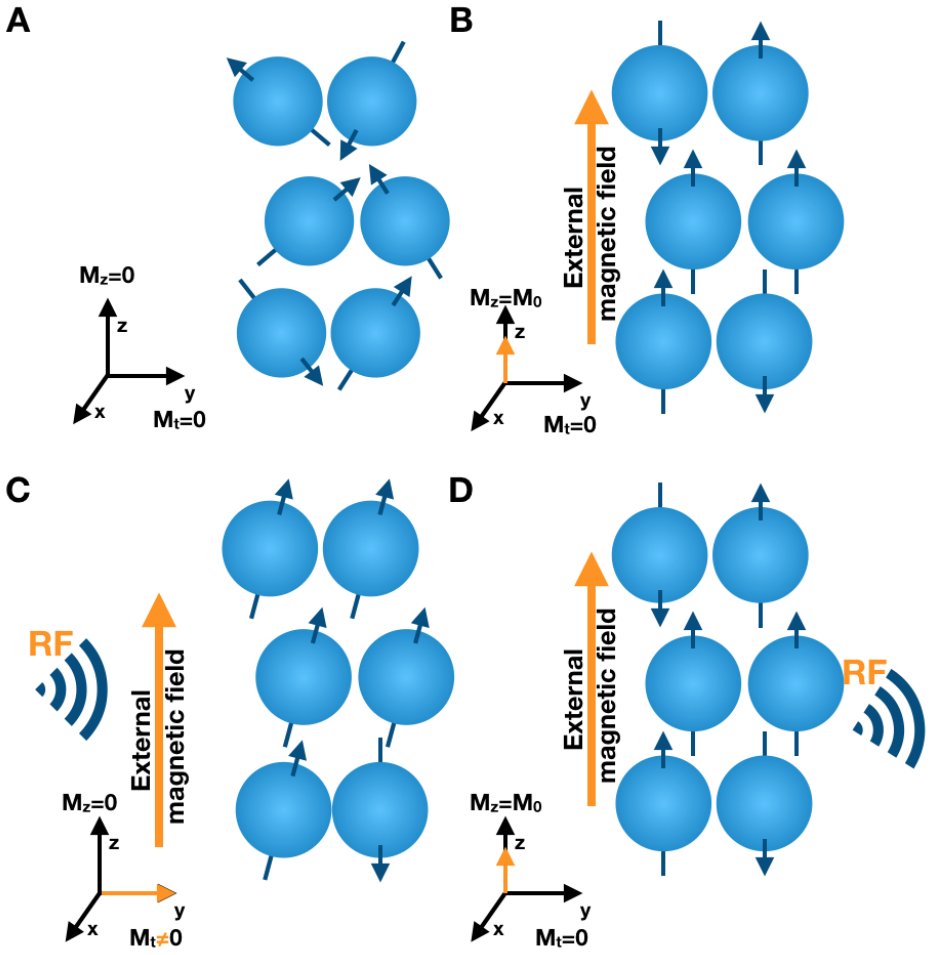

Fig. 1.4: Nuclear magnetization principle of MRI. *(A)* Representation of the magnetic spins of the Hydrogen atomic nuclei. *(B)* In presence of a strong external magnetic field, the magnetic spins align either parallel or anti-parallel to the external field, having a little net magnetization in the direction of the field (Mz), but null perpendicular to it ($Mt=0$). *(C)* When an external RF magnetic field is applied, the spins precess at the frequency of this magnetic field, they dealign from the initial magnetic field and a detectable perpendicular net magnetization is induced ($Mt\sim=0$, $Mz=0$). *(D)* When the external RF magnetic field is turned off, the spins re-align with the external magnetic field, emitting back an RF signal that can be readout and subsequently converted to a meaningful image.

is proportional to the external magnetic field. However, the net magnetization is still 0 because the individual magnetic moments are aligned either in parallel or anti-parallel to the magnetic field. Therefore, it is necessary to apply an additional radio-frequency (RF) magnetic field, perpendicular to the initial external magnetic field, to induce a net magnetization perpendicular to the first external magnetic field. Once the RF magnetic field is turned off, the net magnetization returns to 0, and the magnetic spins emits an RF signal that can be measured for a limited time (Fig. 1.4), during the process referred to as relaxation [Jenkinson and Chappell, 2018].

Relaxation

Relaxation describes the process of the net magnetization returning to alignment with the external magnetic field after the external RF magnetic field is turned off. This magnetization has two components: one transverse component, parallel to the RF magnetic field, and one longitudinal component, parallel to the external magnetic field. Once the external RF magnetic field is turned off, the transverse component of the magnetization decreases while increasing the longitudinal component, while the magnetic spins emits an RF signal that decays rapidly, typically over the course of tens of milliseconds in brain tissues, defined by the *T2* time constant. On the other hand, the time it takes for the magnetic spins to align to the external magnetic field, typically a few seconds, is defined by the *T1* time constant [Jenkinson and Chappell, 2018].

Different brain tissues have different inherent *T2* times, but it is necessary to read out the RF signal at a time when the difference between the signal received from the different tissues is maximal, which is referred to as the echo time (TE). A proper TE maximizes the contrast between the different brain tissues, having a good signal to noise ratio (SNR). Furthermore, the excitation with the external RF magnetic field is repeated several times to obtain whole-brain imaging. The time taken between excitations is the repetition time (TR). Similar to the *T2* parameter, different brain tissues have different *T1* times, hence, each recovers to a different degree during the TR, then, the choice of TR will affect how big a signal is received from them [Jenkinson and Chappell, 2018]. The different combination of these relaxation times produces several types of image contrasts.

Just as different combinations of relaxation times generate multiple anatomical contrasts, changes in the field homogeneity over the time reflect alterations of neural activity in a reliable way, which can be exploited to image changes in the blood-oxygenation level, a principle that underlies the functional contrast in fMRI [Logothetis, 2008].

1.2.2 Blood-oxygen-level- dependent (BOLD) imaging

In functional brain imaging, the blood-oxygen-level-dependent (BOLD) contrast is measured, which depicts differences in blood oxygenation after neural activity. In baseline, oxygenated blood is diamagnetic, i.e. minimally affecting the magnetic field, and paramagnetic, i.e. distorting the magnetic field and increasing the MRI signal, after oxygen consumption. BOLD imaging measures indirectly the brain activity under the principle that neural activity induces a regional increase in cerebral

blood flow, an increase that provides more oxygen than has actually been consumed. Therefore, the net effect of neural excitation is a counter intuitive drop in the deoxyhemoglobin concentration, which results in an increased BOLD signal [Logothetis, 2008] (Fig. 1.5).

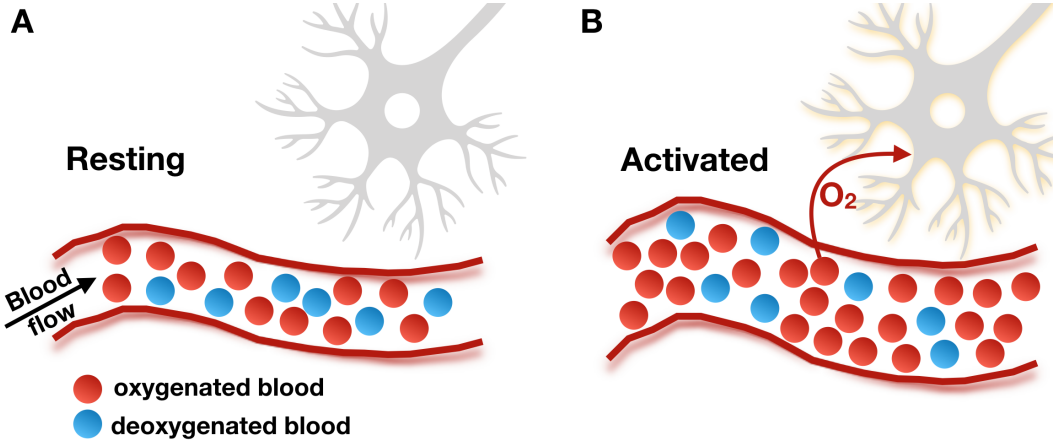

Fig. 1.5: Representation of the BOLD phenomena. Comparing the *(A)* baseline to *(B)* the activated state, a local increase of the neuronal activity induces an increase of the cerebral blood flow, slightly increasing the concentration of oxygen in the blood. Then, the overall amount of oxygenated blood increases, compared to the amount of deoxygenated blood, leading to an increase in the MRI signal.

The *T2** contrast is susceptible to the BOLD phenomena. The rapid acquisition of *T2** weighted images makes possible to detect changes in oxygen consumption, mapping indirectly the neuronal activity. Based on this image contrast, the echo planar imaging (EPI) acquisition technique is commonly used for mapping the BOLD phenomena, due to its short acquisition times and its ability to capture all the image information of one slice with a single RF excitation pulse, in contrast to conventional MRI sequences, where more than one RF excitation pulse is usually needed [Jenkinson and Chappell, 2018].

To improve the spatial and temporal resolution of the EPI images, acceleration techniques are usually used, exploiting the arrangement of multiple coils available in modern RF coils, facilitating the simultaneous acquisition of signals coming from different sources. The most common acceleration technique is the in-plane acceleration image reconstruction method, which acquires partially the image information, synthesizing the missing information based on previously acquired calibration data and the geometric and spatial information of every coil. However, this method only accelerates the acquisition of one slice. Hence, relatively new acquisition acceleration methods known as multiband allow acquiring simultaneously multiple slices.

Multiband-EPI method

Similar to in-plane acceleration methods, multiband-EPI uses the data from different coils to acquire multiple slices simultaneously by exciting them and separating their contributions later on, based on the different local sensitivities of the coils. This method facilitates a considerable shortening of volume acquisition times because the number of simultaneously acquired slices (the multiband factor) directly translates into a reduced number of excitations and thus measurement time (Fig. 1.6). Moreover, both acceleration techniques, in-plane and multiband, can be combined to achieve the advantages of both approaches [Jenkinson and Chappell, 2018].

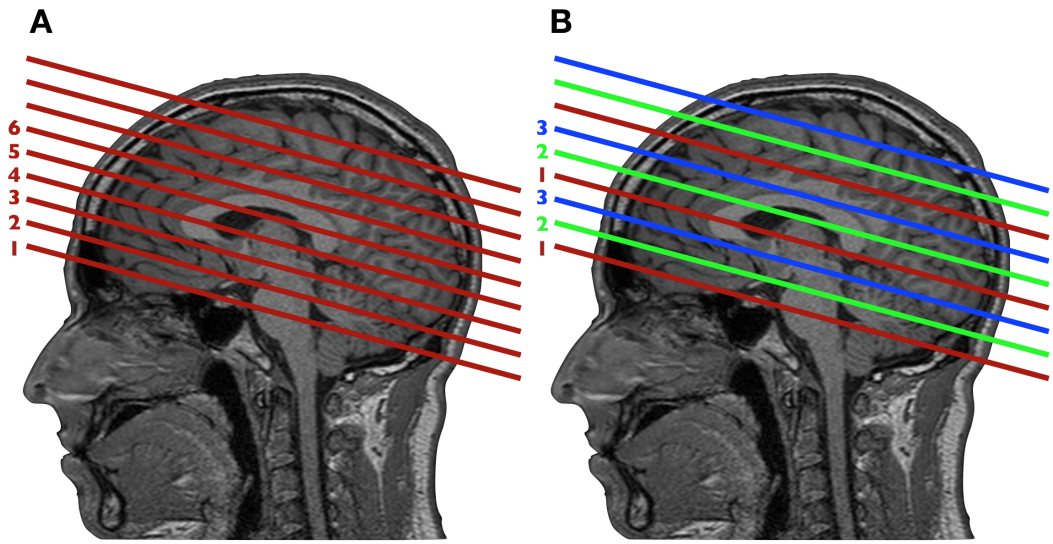

Fig. 1.6: Multiband slice acquisition scheme. *(A)* Conventional ascending slice acquisition. *(B)* Slice acquisition using a multiband factor of 3, where slices with the same color are acquired simultaneously.

1.2.3 Mapping the brain function using the BOLD signal

Based on the BOLD phenomena, fMRI was initially used to map different brain functions while the participants were performing a task or while a stimulus was administered, measuring the changes in neuronal activity related to that performance (task-fMRI). However, fluctuations were also present in the BOLD images, which were not attributed to the experimental task or stimulus but to brain activity that was intrinsically generated by the brain. Resting state fMRI (rs-fMRI) acquires BOLD data while the participant does not perform any task. This data is processed afterward to detect spontaneous or intrinsic neural fluctuations [Fox and Raichle, 2007].

1.2.4 Task based fMRI

In this approach, while the BOLD images are acquired, the participant is asked to perform a task or is exposed to an external stimulus, which is interleaved with periods of rest, where the participant is usually asked to do nothing in particular. The timing of the periods of task and rest are known in advance, and it is referred to as the model. The analysis of task-fMRI involves the correlation of the BOLD time-series with the time-series of the model, which is averaged separately during the periods of task and rest, the average rest-period is substracted from the task-period time-series, highlighting regions modulated by the task [Fox and Raichle, 2007].

1.2.5 Resting state fMRI

Resting state fMRI allows detecting spontaneous neural activity while the participant does not perform any cognitive task in the MRI scanner. Contrary to task-fMRI, where the images acquired during the task/stimulation periods are contrasted with periods of rest to map the brain function, rs-fMRI can be used to observe the functional relationships between different parts of the brain, which have a coherent signal amplitude and temporal fluctuation [Jenkinson and Chappell, 2018]. This signal is not attributable to specific inputs or outputs, instead, it is intrinsically generated by the brain and is organized in large-scale distributed networks, usually referred to as brain intrinsic functionally connected (iFC) networks. There are several alternatives for identifying these iFC networks, an analysis often referred to as brain functional connectivity (FC) [Friston et al., 1993; Fox and Raichle, 2007; Yeo et al., 2011].

Brain functional connectivity

Brain FC refers to the analysis of inter-regional similarities in neuronal variability between anatomically separated brain regions [Fox and Raichle, 2007; Heuvel and Hulshoff Pol, 2010]. Two regions are said to be functionally connected if the time series of their activity are highly correlated, a fact usually interpreted as both regions are likely to be communicating and sharing information [*CPAC website*]. The most commonly used methods to analyze rs-fMRI data are:

- **Seed-based correlation analysis (SCA)**: It consists of extracting the BOLD time series from a region of interest, the seed region, and determine the temporal correlation between this and the time series from all other voxels in the brain [*CPAC website*].

- **Independent component analysis (ICA)**: It decomposes BOLD images into components that are maximally independent in a statistical sense, each of them associated with a spatial map. While some maps reflect noise components others reflect functional brain systems. Therefore, the spatial maps resembling the iFC brain networks (Section 1.2.5) are selected, whereas the noise maps are discarded [Fox and Raichle, 2007].

- **Amplitude of low frequency fluctuations (ALFF)**: It quantifies the amplitude of the slow fluctuations in the BOLD signal, expressed via two metrics, the ALFF, which represents the strength of the low-frequency oscillations, and the fractional ALFF (fALFF), which represents the relative contribution of specific low-frequency oscillations to the whole frequency range [Zang et al., 2007; Zou et al., 2008; *CPAC website*].

- **Regional Homogeneity (ReHo)**: It evaluates the synchronization between the time-series of a given voxel and its nearest neighbors based on Kendall's coefficient of concordance [Zang et al., 2004; *CPAC website*]

- **Graph-based analysis**: It represents the BOLD data as a mathematical graph. The time series for each voxel or group of voxels is extracted and used to calculate a temporal correlation matrix between each pair of time series, a matrix that represents the connectivity between all nodes. Afterward, this graph can be characterized with any of the graph theory metrics and analysis available.

Intrinsic functionally connected brain networks

A key feature of brain organization is the integration of specialized brain regions into large-scale networks. Therefore, brain function research has moved from studying isolated individual brain regions to the interactions and connections between regions. The study of these brain networks has been mostly done using rs-fMRI [Heuvel and Hulshoff Pol, 2010]. Several brain iFC networks can be identified using any of the FC methods described in the section 1.2.5, such as SCA or ICA. Although several brain parcellations based on rs-fMRI data have been proposed, I followed the one suggested by Yeo et al. [Yeo et al., 2011] based on a cohort of 1000 healthy subjects (Fig. 1.7). In this large-scale dataset, the authors identified the following 7 brain iFC networks:

- **Visual (VIS)**: This corresponds to medial and occipital pole, and extrastriate areas. It is related to visual function.

- **Sensory-motor (SM)**: This includes supplementary motor area, sensorimotor cortex, secondary somatosensory cortex, superior temporal gyrus, Heschl's gyrus and posterior insular areas. It is related with sensorimotor and auditory functions.

- **Dorsal attention (DAN)**: This includes superior parietal lobule (SPL), intraparietal sulcus (IPS), frontal eye fields (FEF) and extrastriate areas. It is related with the mediation of goal-directed, top-down attention processes.

- **Salience (SAL)**: This includes dorsoanterior prefrontal cortex (DAPFC), anterior insular cortex (AIC), dorsal anterior cingulate cortex (dACC) and limbic structures. It is related with the integration of external sensory information with internal emotional and bodily state signals.

- **Central executive (CEN)**: This includes dorsolateral prefrontal cortex (DLPFC), rostro-lateral IPS and inferior parietal lobule (IPL) areas. It is related with the mediation stimulus-driven, bottom-up control of attention.

- **Default mode (DMN)**: This includes precuneus, posterior cingulate cortex, bilateral inferior–lateral– parietal and ventromedial frontal cortex. It is most commonly seen as deactivating in task-fMRI studies. It is related with the brain function at rest, episodic memory processes and self-referential mental representations.

- **Limbic**: This includes limbic structures. It is related with emotional processing.

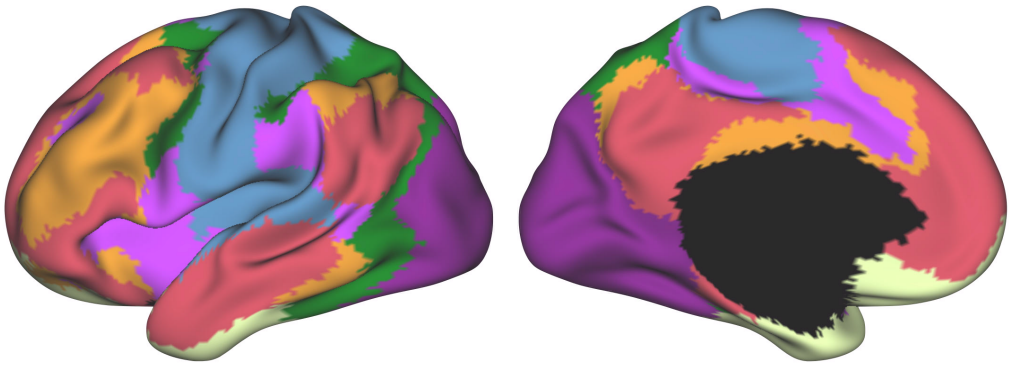

Fig. 1.7: Main iFC brain networks. Brain parcellation derived from 1000 healthy subjects [Yeo et al., 2011]. VIS: purple, SM: blue, DAN: green, SAL: violet, CEN: orange, DMN: pink, Limbic: cream.

1.3 Measuring the effect of TMS on brain function with fMRI

TMS and fMRI are complementary techniques that when combined can compensate for the limitations of either technique used alone [Fox et al., 2012]. By temporarily disrupting ongoing neural activity with TMS, one can evaluate the contribution of the stimulated cortex to a specific brain function with fMRI. Combined TMS-fMRI studies can be classified according to the temporary relationship between both techniques, being *online* if the stimulation is given while scanning, or *offline* if the stimulation is performed outside the MRI scanner [Hartwigsen et al., 2009]. Online TMS is a deterministic approach, where a single or a short train of pulses directly elicit action potentials that may have relatively uniform physiological and behavioral effects. Offline TMS is a neuromodulatory approach, where a longer TMS stimulation modulates ongoing brain activity beyond the duration of stimulation [Polania et al., 2018]. The combination of TMS with fMRI allows us to non-invasively modulate brain activity and measure causal effects on brain imaging measures. TMS effects might vary between individuals, owing to brain-intrinsic differences or methodological factors [Polania et al., 2018]. Certain methodological considerations should therefore be taken into account to minimize the variability in the results of group studies.

1.3.1 Methodological considerations

In order to minimize variability and obtain more conclusive and specific results, combined TMS-fMRI studies should incorporate as many of the following methodological considerations as possible [Fox et al., 2012; Polania et al., 2018]:

- The use of neuronavigation to identify stimulation targets based on the individualized anatomical or functional images of each participant, thereby minimizing between-participants differences.

- The inclusion of control tasks or behavioral measures that ascertain that the stimulation effects are specific for the behavior or function under study.

- To control for as many non-specific effects as possible, varying stimulation frequency, stimulation site, and the networks examined to show maximal specificity of the result.

- The selection of the proper fMRI technique (task or rest) and analysis (SCA, ICA, etc.) which quantify the strength of the TMS effect on the local neural

effect of interest and how remote brain regions are affected by the application of the stimulation.

- To validate the changes found in the brain function and behavior using theory-driven models when available.

1.3.2 Previous Studies

TMS and task-fMRI

Early TMS-fMRI studies were task-based, evaluating e.g. the effect of motor cortex-TMS with measurements of MEP in the periphery [Hartwigsen et al., 2009]. On the level of brain imaging, TMS of motor areas consistently induced effect within [O'Shea et al., 2007; Min et al., 2016] and beyond the motor network [Bestmann et al., 2005; Min et al., 2016]. However, results have been heterogeneous with respect to the direction of induced brain changes. E.g., studies have reported an increase in the BOLD signal using either online excitatory TMS [Bestmann et al., 2005] or offline inhibitory TMS [O'Shea et al., 2007] while others found decreased BOLD responses after offline inhibitory TMS [Min et al., 2016].

O'Shea et al. [2007] studied the short-term reorganization of the motor network after stimulation of the left dorsal premotor cortex (PMd) with inhibitory TMS, disrupting the behavioral performance immediately afterwards and leading to a compensatory increase in right motor areas, but only during task periods of action selection. With similar results, Min et al. [2016] characterized the effect of inhibitory TMS on M1 during a finger-tapping task, observing an increase in the BOLD signal on the stimulated network, but a decrease in other networks. Finally, Bestmann et al. [2005] compared the effect of subthreshold and suprathreshold excitatory TMS on the left PMd, finding an increase of the BOLD signal in the motor network for both stimulation intensities. In summary, TMS robustly modulates the motor network. However, the TMS parameters and fMRI tasks have been heterogeneous, yielding different results particularly with respect to the direction of effects, i.e. both increasing or decreasing brain activity.

In addition to the stimulation of areas in the motor network, other brain networks have been assessed with TMS, such as the VIS [Ruff et al., 2006; Heinen et al., 2014] and the attention networks [Leitao et al., 2015]. The VIS organization was assessed by Ruff [Ruff et al., 2006], stimulating the FEF online with excitatory TMS, observing an increase in the activity of the peripheral visual cortex, but a decrease in the central visual cortex. Similarly, online excitatory TMS of the FEF during a visual

attention task increased the BOLD signal in motion/face areas [Heinen et al., 2014]. Furthermore, the relationship between the attention networks was assessed during a spatial attention paradigm using online high-frequency TMS on the IPS, increasing the BOLD signal in the IPS and in the insula during visual targets, but decreasing it in visual areas [Leitao et al., 2015]. Overall, TMS shows a robust, context-dependant effect on high-cognitive functions. However, studies again largely diverge with respect to the sign of the effect on brain activity. Moreover, the interpretation of these results is confounded by the superposition of both task-evoked activity and resting state fluctuations [Fox et al., 2006; Fox et al., 2012]. Therefore, TMS in combination with rs-fMRI has recently become more popular.

TMS and rs-fMRI

Combined TMS/rs-fMRI studies have evaluated the modulatory effect of TMS on ongoing brain activity, and thus, the stimulation is applied offline. Similar to combined TMS/task-fMRI studies, the modulation of intrinsic activity in the motor network is the most commonly investigated. Nettekoven et al. [2014] assessed the relationship between the MEP and FC response to excitatory TMS on the left M1, finding an increase of both metrics after stimulation. Targeting the same area, Watanabe et al. [2014] observed either an increase or a decrease in the FC after inhibitory and excitatory TMS, respectively, however, with only a small sample size ($n = 6$). In 2015, the same author [Watanabe et al., 2015] tested the top-down relationship between the pre-supplementary motor area (pre-SMA) and basal ganglia structures and reported decreasing FC after inhibitory TMS, but increasing FC after excitatory TMS. In another somatosensory area, Valchev et al. [2015] modulated the primary somatosensory cortex (S1) with inhibitory TMS and found a decrease in contralateral PMd and other sensory areas, extending O'Shea's [2007] results based on task-fMRI. Finally, Cocchi et al. [2015] assessed the changes in the brain global integration after inhibitory and excitatory TMS on the right M1, observing an increase in the within-network FC, but a decrease in the between-network FC.

In addition to the assessment of the motor network, other studies have evaluated the effect of TMS in other sensory networks. Andoh et al. [2015] examined the effect of inhibitory TMS in both auditory cortices and decreased the FC within the AUD and SM networks. Rahnev et al. [2013] characterized the effect of inhibitory TMS on the VIS and found a decrease in the FC within the VIS, however, this study had a small sample size ($n = 5$) and the authors reported a high inter-subject variability on their results. Finally, Cocchi et al. [2016] assessed the effect of inhibitory TMS with rs-fMRI and observed an increase in the FC within the VIS and with frontal areas. In summary, the modulation of sensory networks with TMS seems to have

heterogeneous effects, inducing not only the expected effect in the FC [Rahnev et al., 2013; Nettekoven et al., 2014; Watanabe et al., 2015; Valchev et al., 2015; Andoh et al., 2015] —decreasing it after inhibitory stimulation but increasing it after excitatory stimulation— but also an opposite effect to the expected one [Watanabe et al., 2014; Cocchi et al., 2015; Cocchi et al., 2016]. These heterogeneous results might be attributed to the use of heterogeneous protocols and the stimulation of different areas within the same network, i.e S1 vs. M1, which is the case for both studies by Watanabe at al. [2014; 2015].

The effect of TMS has been also evaluated in high-cognitive networks, where the modulation of the DMN has been the most commonly investigated. Again, findings are heterogeneous, observing both the expected [Werf et al., 2010; Wang et al., 2014; Tik et al., 2017] as well as opposite effects [Eldaief et al., 2011; Chen et al., 2013] on FC. Starting with the first category of studies, Van der Werf et al. [2010] evaluated the effect of inhibitory TMS on the left DLPFC and decreased the FC with the DMN in both temporal lobes and hippocampal areas. Tik et al. [2017] stimulated the same brain region with excitatory TMS for treatment purposes, observing an increase in the FC of the DMN. Finally, Wang et al. [2014] evaluated the effect of excitatory TMS on the lateral parietal cortex and its relationship with memory functions, observing an increase in the FC between the hippocampus and DMN areas.

In the second category of studies, Eldaief et al. [2011] tested the effect of both inhibitory and excitatory TMS on the IPL, observing a decrease in the FC of cortical DMN areas, but not hippocampal areas after excitatory TMS; and an increase in the FC of hippocampal areas, but not cortical DMN areas after inhibitory TMS. Stimulating regions in other brain networks, Chen et al. [2013] studied the causal mechanism by which the CEN and SAL interact with the DMN by using both online-inhibitory and offline-excitatory TMS, inducing an increase and a decrease in the FC between both networks and the DMN, respectively.

In addition to the DMN, the remaining studies have mostly modulated areas within the attention networks CEN and DAN, which are positively correlated with the SAL, but negatively correlated with the DMN [Fox and Raichle, 2007; Glasser et al., 2016]. Two studies found a decrease in the FC after inhibitory TMS [Mastropasqua et al., 2014; Cocchi et al., 2016], but Gratton et al. [2013] found an opposite effect after inhibitory TMS. In the first of these studies, Mastropasqua et al. [2014] evaluated the effect of inhibitory TMS on the right DLPFC of the CEN, observing a within-network decrease in the FC. In a closer area, but within the DAN, Cocchi et al. [2016] tested the top-down relationship between the DAN and VIS networks by stimulating the right FEF, observing a decrease in the FC with the VIS network. Lastly, Gratton et al. [2013] stimulated two brain areas belonging to the CEN and SAL networks and

found an increase in the FC within both stimulated networks and between-network effects with DMN areas. To summarize, TMS does not have a clear and unique effect on high-cognitive networks, mostly because of the complex relationships between the different brain regions conforming a brain network or system, nevertheless, it seems that TMS induced an effect in the FC that is driven by the correlation between the brain areas of interest at baseline.

1.4 Contributions of the thesis

The literature review shows that, firstly, the number of studies using combined TMS and rs-fMRI has been increasing since 2010. Secondly, they have employed heterogeneous methodological procedures (Section 1.3.2). Thirdly, inhibitory TMS is the most commonly used protocol across studies. Fourthly, inhibitory TMS seems to have a variable effect on the FC of different functional networks, with heterogeneous results among studies, especially in high-cognitive networks. Furthermore, some studies using excitatory TMS have reported negative results when combined with rs-fMRI [Bilek et al., 2013; Cocchi et al., 2015] and task-fMRI [Min et al., 2016]. Fifthly, TMS seems to have a different effect depending on a sensory or a high-cognitive area was stimulated, which has yet to be sufficiently accounted for. Finally, to date, most of the studies which have reported between-network findings, have not evaluated their relationship with the global brain function.

In this study, I implemented a modulatory TMS protocol which alters the FC at the brain network level, controlling for as many factors as possible to achieve the most conclusive and specific results (Section 1.3.1). Firstly, I minimized the between-participant variability by locating the TMS target areas based on the individualized functional information derived from the rs-fMRI of each participant. Secondly, I used inhibitory-TMS, the most common protocol used in previous studies (Section 1.3.2), to stimulate three different brain areas: one in a sensory network, one in a high-cognitive one, and the superior-temporal gyrus area to control for nonspecific effects of TMS stimulation. Thirdly, I evaluated the modulatory effects of the stimulation using rs-fMRI, avoiding some of the interpretive difficulties associated with task-fMRI. Finally, using the appropriate FC analysis, I assessed the TMS effect at three different levels: regionally, within the stimulated region, network-wise, in remote brain regions interacting with the stimulated region, and globally, to examine the effects on the global brain network communication.

2 Objectives

TMS can manipulate brain activity in areas beyond the stimulated region. Hence, this method is commonly combined with a brain imaging method to assess their effects on the brain activity. Particularly, fMRI provides crucial information to map the effects of stimulation on a brain system level. This thesis consists of two consecutive projects. The first one evaluates a new fMRI acquisition method to improve the specificity to detect brain network activity. The second project evaluates systematically the effect of TMS on the brain activity and network communication according to the type of brain region stimulated.

2.1 Project 1: Evaluation of accelerated multiband acquisitions for rs-fMRI

Functional magnetic resonance imaging (fMRI) is the method of choice to non-invasively study the brain activity in humans. In order to improve its temporal resolution, new acquisition acceleration methods known as multiband, which are able to acquire several slices simultaneously, have been developed. However, these methods have an effect on the quality of the images, which has not been fully evaluated yet. The objective of this study is to evaluate the effect of multiband acceleration on the image quality and sensitivity to detect brain network activity in fMRI datasets. I hypothesized that multiband accelerated fMRI impacts the image quality, and thus, its sensitivity to detect brain network activity. To test this hypothesis, I acquired multiband accelerated fMRI datasets with different multiband factors (1 to 4) and I compared the image quality parameters (temporal SNR and g-factor) and the brain networks derived from these datasets to the ones obtained with the standard protocol. This study provides an optimized acquisition protocol for multiband-accelerated fMRI with a higher temporal resolution and sensitivity to detect brain network activity without affecting the image quality.

2.2 Project 2: Effect of TMS on the global brain communication depending on the stimulation site

Transcranial magnetic stimulation (TMS) is a promising tool to modulate brain activity non-invasively in humans. However, the influence of TMS on brain activity and communication among sensory and higher cognitive systems is still not fully understood, yielding to heterogeneous findings in the literature. The objective of this study is to evaluate the effect of inhibitory TMS on the brain activity and communication among sensory and higher cognitive systems. I hypothesized that inhibitory TMS has a different effect on the brain activity and communication depending on whether a sensory or a higher cognitive system is stimulated. To test this hypothesis, I applied inhibitory rTMS to the visual network, a sensory system, the salience network, a higher cognitive system, and the superior temporal gyrus, as a control network, to study the effect of stimulation on the local, network and global brain activity with resting state fMRI. This study provides a more specific understanding of the effect of TMS on the brain activity and communication between systems, differentiating the effect on sensory from higher cognitive systems.

3 Materials and Methods

3.1 Project 1

3.1.1 Participants

Twenty healthy participants (11 female, mean age = 24.6 years, SD = 4.1 years) took part in this study. They were informed about the objective and potential risks of the study and signed a written consent inform. The study was approved by the local institutional review board and was conducted in accordance with the Declaration of Helsinki.

3.1.2 Study design

A multiband-EPI sequence (mb-EPI) [Feinberg and Setsompop, 2013] with blipped-controlled aliasing [Breuer et al., 2005; Setsompop et al., 2012] was used. Four rs-fMRI datasets with different M-factors and numbers of volumes (n) were acquired for 7 minutes in order to compare the performance of mb-EPI acquisitions with different slice-acceleration factors. The datasets' repetition times (TR) were near the minimum and flip angles (α) were adjusted to yield the maximum signal (Ernst angle). The participants were instructed to stay awake with their eyes closed, without falling asleep. Furthermore, the acquisition order was permuted between participants to avoid acquisition order bias on the results.

3.1.3 Image acquisition

Experiments were performed on a Philips Ingenia 3T scanner (Philips Healthcare, Best, The Netherlands) using the body coil for transmission and the 32 channel head coil for signal reception.

Functional MRI

All investigated mb-EPI protocols were in-plane accelerated with SENSE [Pruessmann et al., 1999], using an acceleration factor of 2 (S2) since this was observed to reduce susceptibility artifacts with minimal SNR degradation [Dietrich et al., 2007]. A matrix size of 64*x*64, a voxel size of 3*x*3*x*3 mm^3 and 36 slices with a 0.3 mm gap allowed complete brain coverage in most of the participants.

Despite having the same geometric parameters, each protocol had different a acquisition parameters combination (combined one to one) —*M*-factor = 1, 2, 3, 4, *TR* = 2000, 1000, 700, 520 ms and $\alpha = 90°, 70°, 60°, 50°$— yielding to a total of $n = 210$, 420, 610, 810 volumes. These protocols are referred to as *S2*×*M1*, *S2*×*M2*, *S2*×*M3* and S2×M4 in the following. The reconstruction of the multiband fMRI datasets was done offline on a Windows PC using a dedicated reconstruction software based on the SENSE algorithm (developed with ReconFrame, GyroTools, Zürich, Switzerland), whereas the reference experiment (*S2*×*M1*) was reconstructed at the scanner using the standard reconstruction software. Finally, the reconstruction step took up to about 20 minutes depending on the number of volumes.

Structural MRI

Structural MR images consisted of a high resolution T1-weighted 3D-TFE with an isotropic voxel size of 0.7 mm^3, TR of 9 ms, TE of 3.98 ms, flip angle of 8°, 170 slices and FOV of 256 mm. The scan had a duration of 5.9 minutes.

3.1.4 Image quality analysis

To assess the quality of the acquired images, the temporal signal to noise ratio (tSNR) was calculated using SPM8 (http://www.fil.ion.ucl.ac.uk/spm) and in-house written scripts in Matlab (MathWorks, Natick, Massachusetts, USA). Specifically, once the images were reconstructed, they were converted into NIFTI format (.img/.hdr) and consequently corrected for motion using the SPM8 realignment procedure with standard parameters. Then, the motion corrected images were corrected for scanning drift artifacts using quadratic detrending. Finally, the structural T1 images were segmented into gray matter (GM) and white matter (WM) in native space and coregistered to the mean EPI volume generated during realignment for each participant. The segmented GM and WM masks were thresholded using a probability threshold of 0.75.

The voxelwise tSNR (SNR(t)) [33] was calculated based on all four multiband EPI time-series of every participant by calculating the mean $\bar{S}(t)$ and the standard deviation of the signal $\sigma(S(t))$ across the time course according to

$$SNR(t) = \frac{\bar{S}(t)}{\sigma(S(t))}$$

SNR(t) was calculated for the full ($SNR_{full}(t)$) (n = number of volumes) as well as for truncated time-series of 210 volumes ($SNR_{210}(t)$) which were also used for analysis with regard to brain iFC networks.

In addition, the structured and spatially varying noise presented in accelerated parallel imaging, due to residual aliasing, was quantified through the calculation of geometric factor (g) maps derived according to [Breuer et al., 2009]

$$g = \frac{SNR_{full}}{SNR_{acc}\sqrt{R}}$$

where SNR_{full} and SNR_{acc} denote the tSNR of the fully sampled and accelerated images, respectively, while R is the acceleration factor.

Because multiband acceleration methods do not induce directly tSNR penalty related to the achieved acceleration, a signal-leakage factor L [Xu et al., 2013] has been proposed to characterize the structured noise due to residual aliasing. In the current study, I used both multiband and in-plane accelerated imaging, with a reduced TR and flip angle to achieve most efficient sampling for rs-fMRI experiments, then, an apparent g-factor map according to

$$g_{app} = \frac{SNR_{full,M=1}}{SNR_{acc,M>1}}$$

was proposed to assess the increase of structured noise derived from increasing the multiband factor.

3.1.5 Functional connectivity analysis

The FC analysis was carried out in all the datasets (M-factors 1 to 4) using the full time-series (full analysis). The number of volumes was different for every dataset due to the different TR used for every M-factor (M1: 210 volumes to M4: 810

volumes), even though the acquisition duration was the same (420 s). Therefore, I also assessed the reliability of the results with datasets with an equal number of volumes, and thus, having a variable acquisition duration for each M-factor. Based on the number of volumes of the standard no-accelerated acquisition (210 volumes), the FC analysis was carried out on subsets of the first 210 volumes for each M-factor (truncated analysis).

The pre-processing of the fMRI datasets was carried out using FEAT (fMRI expert analysis tool) version 6.00, part of FSL (FMRIB Software Library, www.fmrib.ox.ac.ukfsl) and included, first, the motion correction of the images using MCFLIRT (motion correction FLIRT - FMRIB linear image registration tool) [Jenkinson et al., 2002], followed by the removal of the non-brain tissue using BET (brain extraction tool) [Smith, 2002], and the spatial smoothing using a Gaussian kernel with full width at half maximum (FWHM) of 6.0 mm. Furthermore, the spatial-smoothed images were normalized with respect to the grand-mean intensity of the entire 4D dataset, then high-pass filtered (Gaussian-weighted least-squares straight line fitting with $\sigma = 62.5$ s) and, finally, they were registered to the standard MNI 152 brain (spatial resolution 2 mm) using FLIRT [Jenkinson and Smith, 2001; Jenkinson et al., 2002].

The FC analysis was carried out separately for both the full and the truncated datasets using FSL MELODIC (multivariate exploratory linear decomposition into independent components) version 3.14. The pre-processed datasets of all participants and multiband factors (M1 to M4) were temporally concatenated, whitened and projected into a 70 dimensional subspace using principal component analysis. The whitened observations were decomposed into sets of vectors describing signal variations across the temporal, session, participant and spatial domain by optimizing for non-Gaussian spatial source distributions using a fixed-point iteration technique [Hyvärinen, 1999]. Finally, a set of 70 spatial maps were generated, which were divided by the standard deviation of the residual noise and thresholded by fitting a mixture model to the histogram of intensity values [Beckmann and Smith, 2004].

The group-average set of spatial maps derived from the ICA were used to generate the individual spatial maps with their correspondent time-series, using dual regression [Beckmann et al., 2009; Filippini et al., 2009]. First, for each participant, the group-average set of spatial maps was regressed (as a spatial regressor in a multiple regression) into the single participant 4D space-time dataset. This resulted in a set of participant-specific time-series, one per group-level spatial map. Then, those time-series were regressed as temporal regressors, again in a multiple regression, into the same 4D dataset, resulting in a set of participant-specific spatial maps, one per group-level spatial map. Finally, the functionally relevant components were selected by visual inspection referring to an established baseline set of brain iFC networks [Allen et al., 2011].

3.1.6 Statistical analysis

The individual maps generated from the FC analysis were used to test for differences in the spatial extent (factor: number of voxels) and the stability of the networks (factor: peak Z-score) across M-factors (factor: M) in a repeated-measures ANOVA model. The post-hoc paired t-tests were carried out using the FSL randomize permutation-testing tool [Winkler et al., 2014] using 5000 permutations ($p<0.001$). This analysis was performed separately for the full and truncated datasets.

3.2 Project 2

3.2.1 Participants

Twenty seven healthy participants (fourteen females, mean age = 25.56 years, SD = 3.01 years), right handed and without any psychiatric condition, were informed about the objectives and potential risks of the study and signed a written consent inform. The study was approved by the local institutional review board (registration number: 221/15S) and was conducted in accordance with the Declaration of Helsinki.

3.2.2 Study design

Each participant underwent three counterbalanced TMS-fMRI sessions on different days, where one of three brain networks — salience network: SAL, visual network: VIS, superior temporal gyrus: Control network — was stimulated with TMS (section 3.2.3). Each session consisted of a baseline rs-fMRI (pre-TMS), followed by 20 minutes stimulation outside the MRI scanner (offline TMS approach) and a rs-fMRI post-TMS to read out the effect of the stimulation (Fig. 4.4). The time between the end of the stimulation and the start of post-TMS rs-fMRI acquisition was kept as short as possible, trying to have an immediate read out of the TMS effect (mean = 5.87 min, SD = 1.1 min). During all rs-fMRI acquisitions, the scanner room was dimmed and the participants were asked to stay awake with their eyes open, without falling asleep. This was ensured by monitoring their eyes with an MR-compatible infrared camera (12M, MRC Systems, Heidelberg, Germany) installed on the coil. The structural MR images acquired during the first pre-TMS session were transferred into the stereotactic TMS system for stimulation (Section 3.2.3), whereas the functional MR images were used for the selection of the individualized TMS target areas (section 3.2.4).

3.2.3 Brain stimulation

Transcranial magnetic stimulation (TMS) was delivered using a Nexstim eXimia system (version 4.3; Nexstim Plc, Helsinki, Finland) in combination with a biphasic figure-of-eight shaped stimulation coil [Sollmann et al., 2016]. Before every TMS session, the neuronavigation system was set up by co-registering the participant's head to its structural MR images, in order to localize the coil position with respect to the individual anatomical structures. TMS target areas were derived from the first functional scan (see below) and then overlaid onto structural images to achieve individual target stimulation.

Low-frequency repetitive navigated TMS (rTMS) with a frequency of 1 Hz and a stimulation intensity of 100% of the individual rMT (further details following, mean rMT = 34.4 %, SD = 7.5 %) was applied during 20 minutes to one of the stimulation targets (1200 rTMS pulses in total) outside of the MRI scanner. During stimulation, the coil was angulated perpendicular to the skull surface, and anterior-posterior orientation of the induced electric field was maintained throughout using an adjustable coil holder (Fig. 3.1).

TMS resting motor threshold (rMT)

During the first session, the resting motor threshold (rMT) was determined after the co-registration step, according to the maximum likelihood algorithm by motor mapping of the cortical representation of the right abductor pollicis brevis muscle, using surface muscle electrodes [Neuroline 720; Ambu, Ballerup, Denmark] and an integrated electromyography device [Awiszus, 2003; Rossini et al., 2015; Sollmann et al., 2016].

3.2.4 Image acquisition

Magnetic resonance images were acquired on a Philips Ingenia 3T scanner (Philips Healthcare, Best, The Netherlands) using the body coil for transmission and the 32 channel head coil for signal reception. The structural MRI was acquired before TMS stimulation, while rs-fMRI was acquired both before and after.

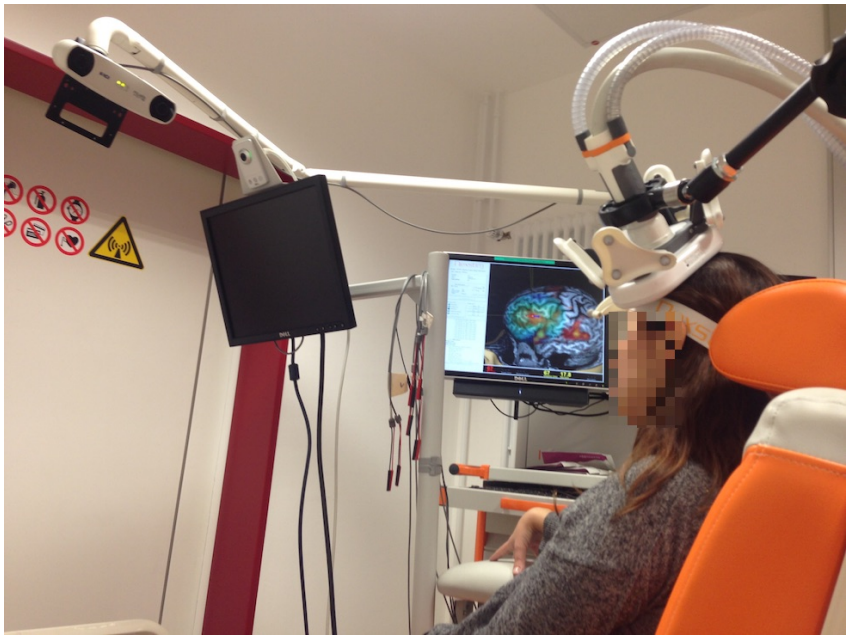

Fig. 3.1: TMS stimulation setup. After the baseline TMS, participants were stimulated for 20 minutes outside the MRI scanner. The TMS stimulation was navigated based on the participant structural images taken during the first session (3D-representation in the monitor) and an optical tracking system based on infrared cameras (upper left). The TMS system was located next to the MRI scanner (the MRI scanner door can be seen in the left of the photo) to minimize the time between the end of the stimulation and the post-TMS rs-fMRI acquisition.

Resting state functional MRI

Functional MR images consisted of a multiband EPI acquisition [Preibisch & Castrillon et al., 2015] of 40 slices and 600 volumes, with an isotropic voxel size of 3 mm^3, multiband factor of 2, SENSE factor of 2, repetition time of 1.25 s, echo time of 30 ms and a flip angle of 90°. The scan had a duration of 12.35 minutes.

Structural MRI

Structural MR images consisted of a high resolution T1-weighted 3D-TFE of 170 slices with an isotropic voxel size of 0.7 mm^3, TR of 9 ms, TE of 3.98 ms, flip angle of 8°, and FOV of 256 mm. The scan had a duration of 5.9 minutes.

3.2.5 Image analysis

Pre-processing

The pre-processing of the structural and functional MRI data was done with version 0.392 of the congurable pipeline for the analysis of connectomes (C-PAC, Craddock et al., 2013).

Structural pre-processing: The structural images were skull-stripped using AFNI-3dSkullStrip, segmented into three tissue types using FSL-FAST and constrained into the individual participant tissue segmentations from standard space provided with FSL. They were then normalized to the Montreal Neurological Institute (MNI) 152 stereotactic space (2 mm^3 isotropic) with linear and non-linear registrations using FSL-FLIRT and FSL-FNIRT, respectively.

Functional pre-processing: The functional images were realigned, motion corrected to the average image using AFNI-3dvolreg, and then skull-stripped using AFNI-3dAutomask. Subsequently, the global mean intensity was normalized to 10000, the nuisance signal was regressed, and the signal was bandpass filtered (0.01 - 0.1 Hz). Furthermore, the pre-processed images were registered to the structural space with FSL-FLIRT using a linear transformation based on the white matter boundary information derived from the prior white matter tissue segmentation from FSL-FAST. Finally, the previous structural to standard space registration was applied to the functional data in order to transform them into the standard MNI space.

The nuisance signal regression step modeled the scanner drift using quadratic and linear detrending, the physiological noise was modeled using the 5 principal components with highest variance from a decomposition of white matter and CSF voxel time-series (CompCor, Behzadi et al., 2007), which were derived from the prior tissue segmentations transformed from anatomical to functional space. Furthermore, the head motion was modeled using the 24 regressors derived from the parameters estimated during motion realignment based on the Friston 24-Parameters, the six head motion parameters and its 12 corresponding squared values.

Image quality assessment: To assess the quality of the acquired images, the images signal to noise relationship and the motion of the participants during the acquisition were estimated through the metrics temporal SNR (tSNR) and framewise displacement parameter (FD). The FD metric was derived from the motion parameters calculated during the pre-processing.

Selection of the TMS target areas

Based on the functional images acquired during the first session, an ICA was carried out on the pre-TMS rs-fMRI data using FSL-MELODIC [Beckmann and Smith, 2004], which decomposed the dataset into 17 different spatial components, following Yeo et al. 2011 [2011] result. Then, the cross-correlation between each ICA map and the Yeo-17 network of interest was computed. The ICA map with the highest cross-correlation value was chosen as the target network. Finally, the TMS target area was extracted from the selected network of interest (the left dorsoanterior prefrontal cortex, DAPFC, in the SAL, the left occipital pole in the VIS and the superior temporal gyrus as a control network) and transfered onto the TMS system (Fig. 4.5).

Functional connectivity analysis

Baseline FC: To characterize the baseline functional images and the connectivity profile of the TMS target areas, an average-group FC map of the stimulated brain networks was generated by running a one-sample t-test on the individual pre-TMS brain FC maps across subjects (Section 3.2.5). Additionally, the session-specific between-network functional connectivity was examined on the same data by computing the Pearson correlation between every pair of average time-series of the stimulated brain networks.

Regional analysis: To evaluate the regional effect of TMS on the brain activity of the stimulated brain areas, the fractional amplitude of low-frequency fluctuations (fALFF) and the regional homogeneity (ReHo) metrics were calculated based on the functional pre-processed images. The fALFF maps were calculated by computing the variance of the bandpass filtered (0.01 - 0.1 Hz) time-series divided by the variance of the non-filtered data, while the ReHo maps were calculated based on the Kendall's correlation between each voxel's time-series and the time-series of the 27 voxels in contact with that voxel. Both measures were calculated in original space and subsequently transformed into the standard MNI space, Z-score transformed and spatial smoothed by a Gaussian kernel with a Full Width Half Maximum (FWHM) of 6 mm^3.

Network analysis: To evaluate the effect and extent of TMS on the brain networks, a seed-based correlation analysis (SCA) was carried out on the functional pre-processed images. The FC maps were based on the correlation between the average time-series of the stimulated brain networks and the time-series of all grey matter voxels in the whole brain. The seeds used for this analysis were based on the Yeo 17-networks parcellation atlas [Yeo et al., 2011]. The FC maps were registered to

the standard MNI space, Z-score transformed and spatial smoothed by a Gaussian kernel with a FWHM of 6 mm^3.

Brain graph modularity analysis : To further understand the effect of TMS, the network findings were extended to a global level by carrying out a graph based consensus modularity analysis of the global FC among cortical nodes of all relevant brain networks [Lancichinetti and Fortunato, 2012; Fornito et al., 2012; Dwyer et al., 2014]. The consensus modularity analysis allows us to derive a group level modular decomposition without losing the inter-individual variability in the network organization [Dwyer et al., 2014]. This analysis was implemented with MATLAB 2015b and the Brain Connectivity Toolbox (Rubinov and Sporns, 2010, https://sites.google.com/site/bctnet). To further interpret the global integration changes, the structural density and modular information of the co-classification matrices was assessed visually by using the force-directed layout representation ForceAtlas2 (Gephi, Jacomy et al., 2014), which depicts the spatialization process of a graph.

At the individual level, the average time-series of 5 mm radius spheres centered on 77 cortical nodes defined by Power et al. [Power et al., 2011] and located on the brain networks affected by TMS on the FC analysis (VIS, SAL, DMN, DAN and CEN) based on their Yeo 17-networks parcellation atlas [Yeo et al., 2011] definition were extracted. Then, a connectivity matrix based on the pairwise Pearson correlation coefficient between every pair of time-series was calculated, the negative correlation values were discarded and the correlation values were transformed to Z-score values. Finally, the community detection Louvain algorithm [Blondel et al., 2008] was ran 1000 times (Fig. 3.2A), in order to deal with the degeneracy problem of this method [Good et al., 2010], generating an individual co-classification matrix, representing the frequency that nodes were co-classified in the same module across iterations (Fig. 3.2B).

At the group (TMS session) level, the individual co-classification matrices were subjected to a second-level modular decomposition, generating a co-classification matrix for each TMS condition (Fig. 3.2C), where two regions consistently co-classified in the same module across participants were assigned to the same module. Furthermore, to understand the functional role of each module and their nodes, the consistency and diversity with which each node was classified into distinct modules was computed based on the group co-classification matrices. The classification consistency (z) quantifies how frequently a node was classified in the same module across participants relative to other nodes in the same module, whereas classification diversity (h) quantifies the variability of each node's modular affiliation across participants [Fornito et al., 2012; Dwyer et al., 2014]. Therefore, brain regions with high z values represent core components of their module, acting as local connectivity

hubs and supporting functional specialization, while brain regions with high h represent transitional nodes, facilitating functional integration between modules [Van Den Heuvel et al., 2008; Rubinov and Sporns, 2011; Fornito et al., 2012; Dwyer et al., 2014].

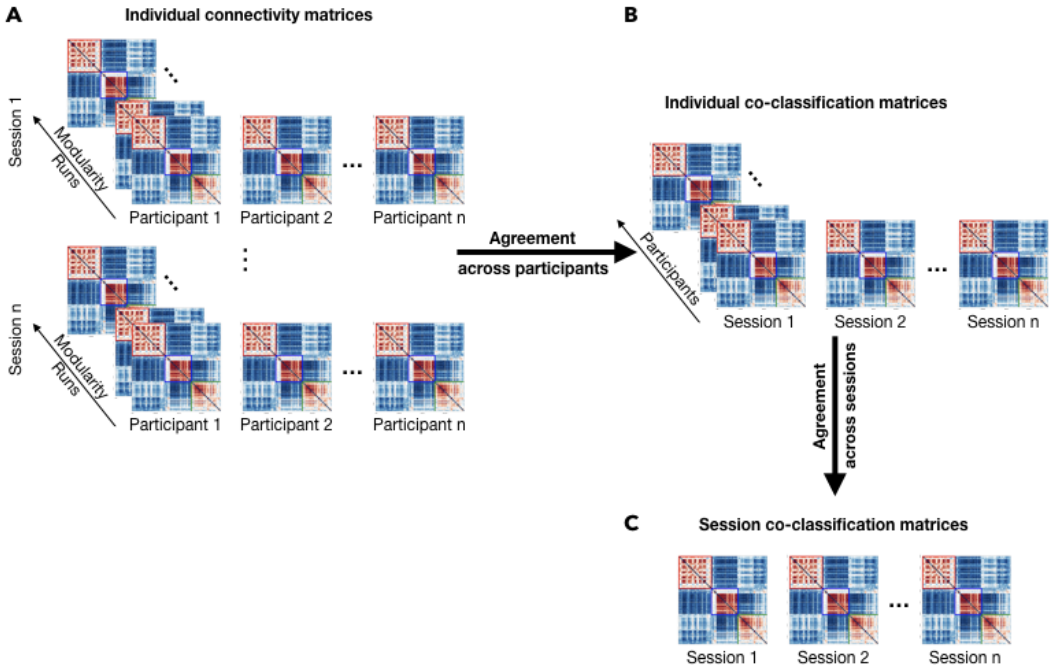

Fig. 3.2: Consensus modularity analysis. The community detection algorithm was run 1000 times on the *(A)* individual connectivity matrices, generating one *(B)* co-classification matrix per participant based on the consensus derived from the 1000-runs partitions. Each element of this matrix represents the proportion of times that two nodes were co-classified within the same module across the 1000 repetitions. Then, one *(C)* session co-classification matrix was generated based on the individual co-classification matrices, where each element of the matrix represents the proportion of times that two nodes were co-classified within the same module across participants in the same session.

3.2.6 Statistical analysis

Voxelwise analysis

I tested for regional and network differences due to TMS by carrying out a voxelwise one-way repeated measures ANOVA on the fALFF, ReHo and FC smoothed Z-score maps using SPM 12 (http://www.fil.ion.ucl.ac.uk/spm). A flexible factorial design was configured with subjects as between-subject factor and TMS-session as within-subject factors with average pre-TMS, VIS-, SAL- and control-TMS as levels. The results were masked using an average gray matter mask derived from all participants. Statistic images were assessed for cluster-wise significance using a cluster-defining

threshold of $p = 0.001$. The critical cluster size was set at $p < 0.05$, FWE-corrected at the cluster level for multiple comparisons.

Modularity analysis

I tested that the modularity analysis results were significantly more modular than expected by chance in three ways, at the level of each participant functional connectivity matrix, at the level of each participant consistency matrix and at the group-level [Dwyer et al., 2014]. For both participant levels, I generated 5000 times a random matrix per participant that matched the empirical matrix for degree, strength, and sign distributions. Each time I ran a modularity analysis (Section 3.2.5, generating a null distribution of median Q values against which the magnitude of the observed sample median Q per condition was compared. Observed sample median Q values were more modular than expected by chance when the $p < 0.05$ [Rubinov and Sporns, 2011; Dwyer et al., 2014; Fornito et al., 2016].

Furthermore, I used a Wilcoxon signed-rank test to evaluate the effect of TMS on the classification consistency and classification diversity values across conditions, with $p < 0.05$ considered statistical significant.

4 Results

4.1 Project 1

4.1.1 Image quality assessment

The EPI is the gold standard method used for fMRI applications. The development of multiband acceleration methods which allows acquiring multiple slices simultaneously has sped up the acquisition times of EPI, optimizing the temporal and spatial resolution of fMRI. Nevertheless, by decreasing the acquisition times, the quality of the image also decreases, therefore, it is important to assess what is the combination of image parameter that combined with an optimal acceleration factor, has the minimal impact on the image quality, increasing its sensitivity to detect brain network activity.

To assess the effect of increasing the multiband factor (M) on the image quality and sensitivity to detect brain network activity, the temporal SNR (SNR(t)) and geometry factor (g) of multiband rs-fMRI datasets acquired using different M-factors was calculated. Overall, there were no significant changes on the image quality metrics up to an M-factor of 2, whereas M-factor bigger than 2 produced random image artifacts. Compared to the reference S2×M1 experiment, experiment S2×M2 had almost the same SNR(t) (Fig. 4.1A) and apparent g-factor (Fig. 4.1C) distributions. Furthermore, the g-factor distribution for the experiment S2×M1 was almost symmetrical around the value of 1, such as the reference S2×M1 experiment. The first two columns of the Figs. 4.1B - D show the SNR(t) and g-factor maps for the reference S2×M1 and S2×M2 experiments. Both metrics maps are very similar for both experiments. In addition, the g-factor map has an overall low-value close to 1, which is the reference value for this metric.

For M-factor values bigger than 2 (S2×M3 and S2×M4), the SNR(t) dropped (Figs. 4.1A - B), whereas the g-factor increased (Figs. 4.1C - D). In addition, some random artifacts appeared on the image quality maps. For the experiment S2xM3, the g-factor maps presented focal spots of noise enhancement that occurred randomly across participants and affected between four and ten slices (Figs. 4.1D: 3rd column, bottom row). Strong, weak or no focal noise enhancement was seen in eleven, six

and three participants, respectively. For the experiment S2×M4, the changes were more evident in both image quality metrics, having a severe drop of SNR(t) (Figs. 4.1A - B) and increase of g-factor (Figs. 4.1C - D), due to a massive increase of structured noise, especially in the center of the brain, which is evident in the SNR(t) and g-factor maps on Figs. 4.1B - D (4th column).

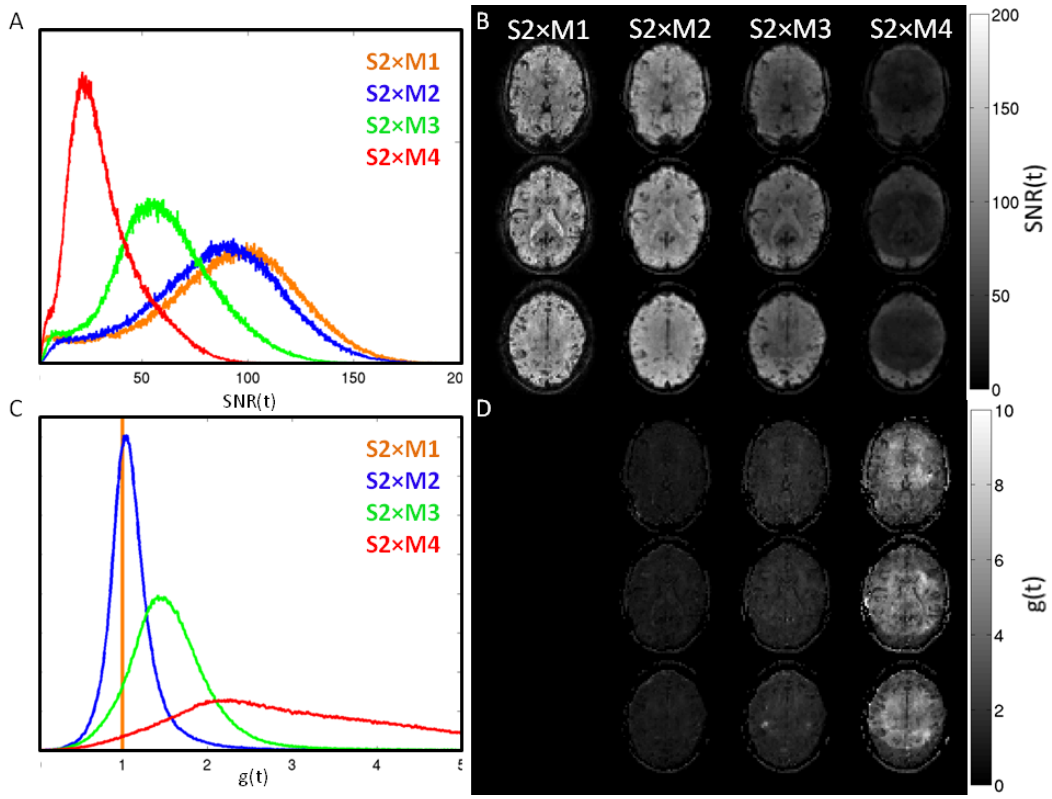

Fig. 4.1: Effect of multiband acceleration on the image quality. Quantitative evaluation of the image quality metrics is presented as histograms of *(A)* SNR(t) and *(C)* apparent g-factor, which are shown together with their respective maps (*(B)* SNR(t) and *(D)* g-factor) of the same slices as in Fig 1. The histograms represent the whole brain data averaged across all 20 participants. On a first glance, the images look similar. However, a more detailed look reveals that the images get degraded with increasing the M-factor. Image taken from Preibisch & Castrillon et al. [2015]

Finally, the truncated datasets had similar image quality metrics compared to the full ones. Table 4.1 summarizes the participant averages of SNR(t) for truncated and full data as well as the apparent g-factors, which were derived from $SNR_{full}(t)$. Moreover, SNR(t) values are tabulated separately for GM and WM, demonstrating that the SNR(t) is generally higher in WM than in GM, except for experiment S2×M4. $SNR_{full}(t)$ and $SNR_{210}(t)$ both show a similar decrease for higher multiband factors. For S2×M2, $SNR_{full}(t)$ and $SNR_{210}(t)$ amount to 93% and 94% of the reference experiment S2×M1 which decreases to 67% and 68% for S2×M3 and goes down to 36% for S2×M4.

Tab. 4.1: Participant averages (mean (std)) of SNR(t) and g-factor for different multiband factors as determined in GM and WM VOIs. All measures were derived from realigned and detrended time-series data.

	S2xM1		**S2xM2**		**S1xM3**		**S2xM4**	
	GM	**WM**	**GM**	**WM**	**GM**	**WM**	**GM**	**WM**
$SNR_{full}(t)$	83.2 (8.5)	98.8 (9.2)	78.1 (9.2)	90.2 (9.2)	58.6 (7.0)	60.2 (7.1)	33.4 (3.8)	28.7 (3.6)
$SNR_{210}(t)$	83.2 (8.5)	98.8 (9.2)	79.1 (8.5)	90.9 (8.9)	59.8 (6.3)	61.1 (6.9)	34.2 (3.7)	29.1 (3.6)
g-factor	1.00	1.00	1.08 (0.09)	1.12 (0.06)	1.46 (0.20)	1.73 (0.20)	2.74 (0.32)	3.97 (0.32)

4.1.2 Functional connectivity analysis

In addition to the qualitative and quantitative evaluation of the temporal and spatial signal behavior of the multiband EPI time-series, the sensitivity of the four mb-EPI protocols to detect brain iFC networks was assessed on the basis of coherent BOLD-signal fluctuations. Overall, mb-EPI acquisition increased the sensitivity to detect the brain iFC networks of interest with increasing M-factor up to 3. For each approach separately, the full and truncated datasets, the 10 most relevant iFC networks were identified using pICA and a voxel-wise ANOVA was carried out to test for differences in the spatial extent of the 4 M-factor maps for each iFC network.

The brain iFC networks were stable across M-factors up to the S2xM3 for both the full and truncated datasets. Only for M4, the ANOVA illustrates increased variability in almost all networks (pink voxels in red networks of S2xM4, Fig. 4.2 last-column), even in the full approach with 4 times the amount of data volumes. It is important to note that the truncated S2×M3 mb-EPI time-series is sensitive enough to detect all relevant iFC networks in only about one third of the total acquisition time. While the acquisition time for the S2×M3 dataset (210 volumes) was 147 s, for the S2×M1 dataset was 420 s.

Finally, to evaluate the differences in network stability across M-factors, the spatial extent, which is the number of voxels in a iFC network with a Z-score > 3, and the signal amplitude, which is the peak Z-score for a given brain iFC network, was quantified. For the full datasets, a significantly improved network sensitivity for both metrics in all M-factors compared to the reference S2xM1 was found (Fig. 4.3A - C). However, for S2xM4, the peak Z-score had a wide error margin reaching partly down to the range of S2xM1.

The Figs. 4.3B - D show the results for the truncated datasets with an identical number of 210 volumes acquired in a decreasing amount of time. These plots indicate that in contrast to the increased stability with higher M-factors as identified in the full dataset, the number of voxels and maximum Z-score rather decreased for the truncated data due to shorter acquisition time. Particularly, S2xM4 significantly

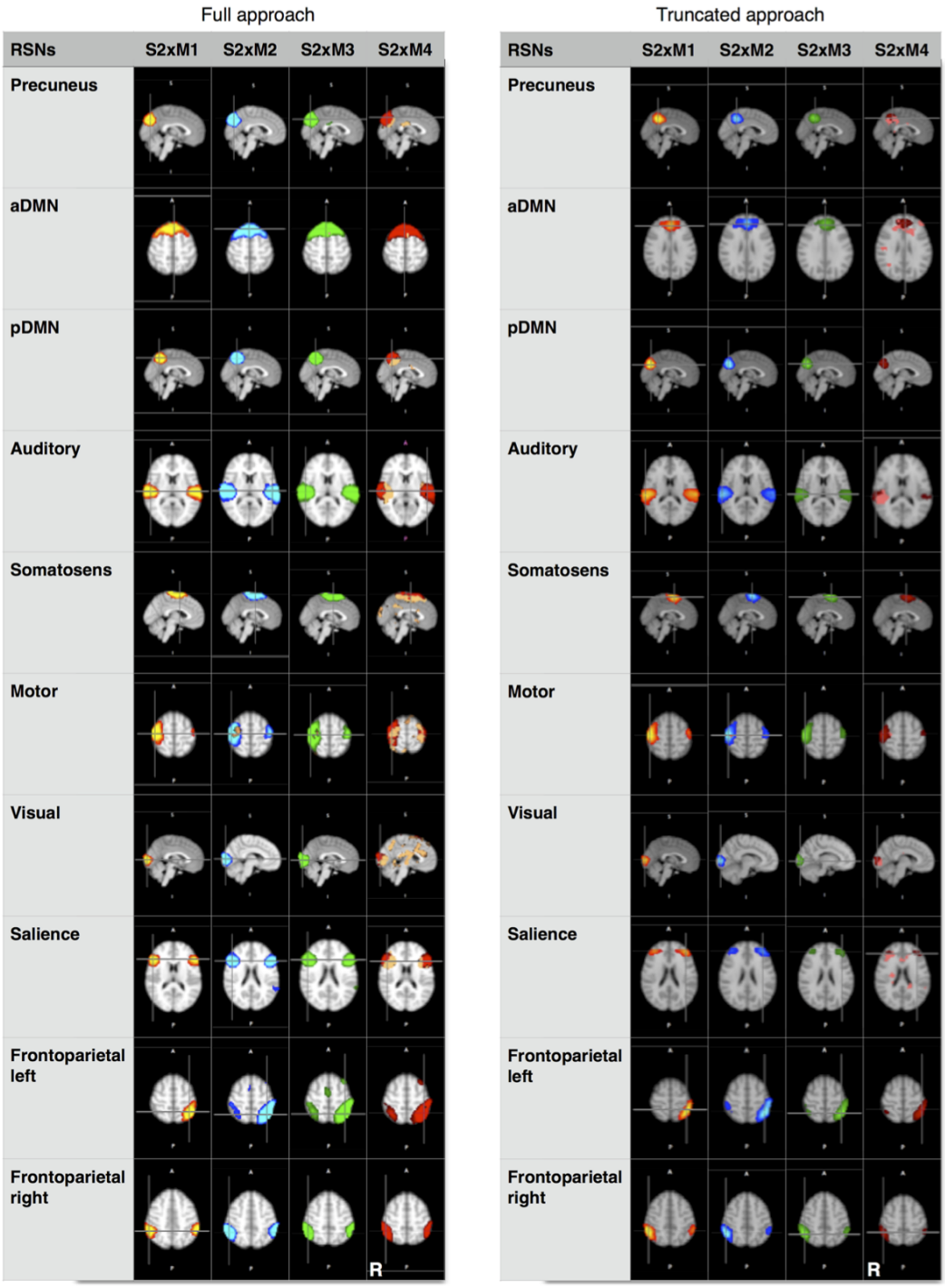

Fig. 4.2: Spatial representation of the ten representative iFC networks. One-sample t-test maps of the 10 iFC networks for each M-factor of the full (left column) and truncated analysis (right column). Voxel-wise differences in the stability of the iFC networks compared to M1 are plotted in pink for each network ($p<0.05$, corrected for threshold-free cluster enhancement (TFCE)). Image taken from Preibisch & Castrillon et al. [2015].

decreased the sensitivity for detecting iFC networks in terms of spatial extent (Fig. 4.3B) and maximum Z-score (Fig. 4.3D). However, as the results of S2xM2 indicates, it seems possible to detect all relevant iFC networks with almost equal sensitivity in only half the acquisition time. Even with S2xM3, all relevant iFC networks (Fig. 4.3B, right column) were detected in full spatial extent, but decreasing significantly its peak Z-score.

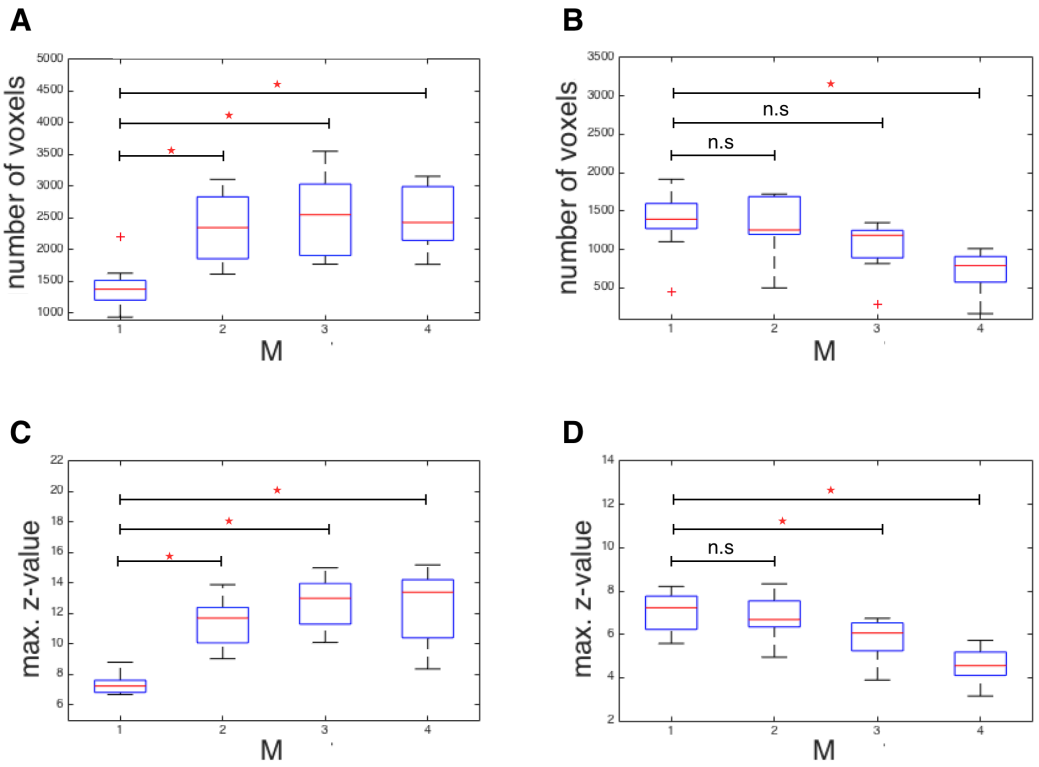

Fig. 4.3: Spatial extent network stability across M-factors. Total number of voxels across all networks for the *(A)* full and the *(B)* truncated datasets and peak Z-score across all networks for the *(C)* full and the *(D)* truncated datasets. Significant differences are marked with an asterisk ($p < 0.001$, repeated-measures ANOVA). Image taken from Preibisch & Castrillon et al. [2015]

4.2 Project 2

Twenty-seven healthy participants took part in three separate TMS/rs-fMRI sessions distributed on separate days. The study design is shown in Fig. 4.4. The intensity used for TMS was based on the individual rMT determined during the first session and then used in the remaining sessions (mean rMT = 34.3% of the TMS system maximum output, SD = 7.6 %). The location of the stimulated target areas was derived from the independent component analysis (ICA) of the individual rs-fMRI images acquired on the first session. The exact location of every participant target area is shown in Fig. 4.5. The time between the last TMS pulse delivered to the

participant and the subsequent rs-fMRI acquisition was kept as short as possible (mean= 5.87 min, SD = 1.1 min). After the exclusion of two participants who did not attend all TMS sessions, and two others due to the extreme location of their SAL target area, twenty-three participants (twelve females, mean age = 25.74 years, SD = 3.22 years) were included in all analysis.

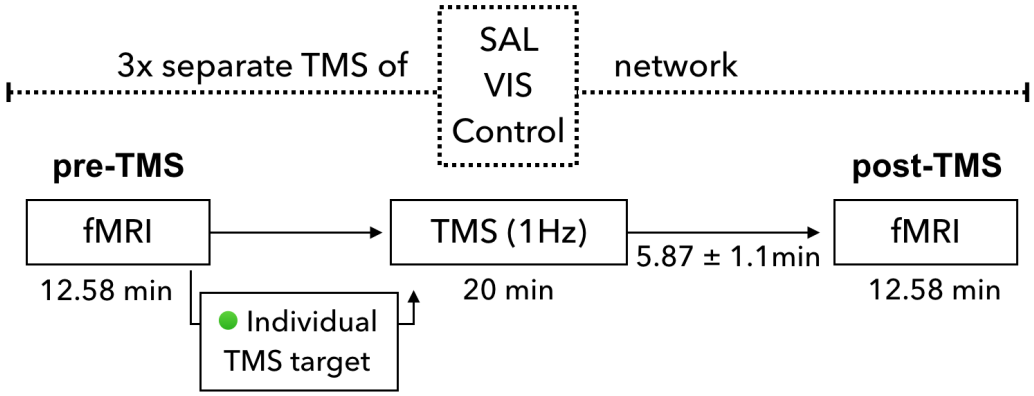

Fig. 4.4: Study design. Repetitive (1Hz) TMS was applied to one of three brain networks (salience network: SAL, visual network: VIS, superior temporal gyrus: Control network) of healthy participants in a counterbalanced fashion on three different days. During each TMS session and for each participant separately, the FC networks derived from the rs-fMRI data (pre-TMS) were identified, and the individual coordinates of the targeted network node were transferred to a stereotactic TMS system for stimulation. Finally, another rs-fMRI dataset (post-TMS) was acquired immediately (mean time delay across all participants = 5.87 min, SD = 1.1 min) after finishing stimulation

4.2.1 Image quality assessment

To avoid bias due to differences in participants motion or image quality parameters across TMS sessions, the FD and SNR(t) metrics were calculated, respectively. The FD across participants (global mean FD = 0.13 mm, SD = 0.03 mm) was within the accepted range (FD < 0.2 mm, Power et al., 2014), without differences across sessions ($p > 0.05$, Bonferroni corrected for multiple comparisons). Likewise, the SNR(t) was stable across participants (global mean SNR(t) = 6.6 a.u, SD = 1.0 a.u), without differences across sessions ($p > 0.05$, Bonferroni corrected for multiple comparisons). Overall, no significant differences were observed for neither the FD nor SNR(t) across TMS sessions (Fig. 4.6).

4.2.2 Baseline functional connectivity

To characterize the FC within and between the modulated brain networks at baseline, the FC maps, and their respective time-series were used to examine the consistency

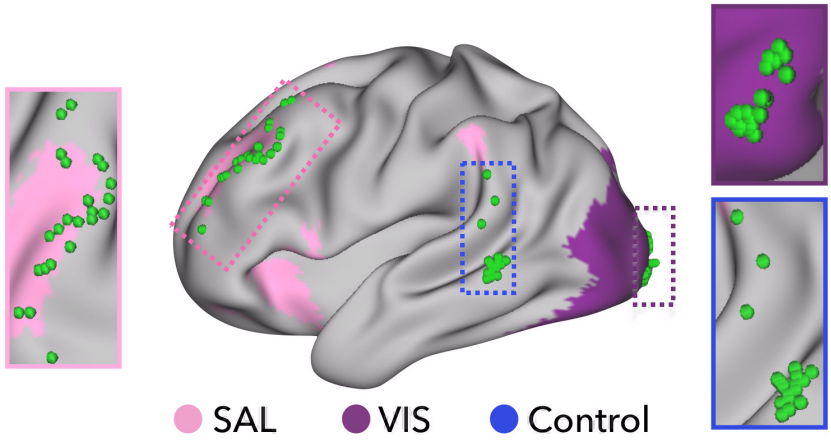

Fig. 4.5: Individual TMS targets areas. Individual targets areas (green spheres) are projected onto the cortical surface of a standard brain and inserts provide perpendicular views of each network node separately. Colored outlines illustrate the average extent of targeted brain networks (pink: SAL, violet: VIS) as identified in a cohort of 1000 healthy subjects by Yeo et al. [2011].

of the brain iFC networks stimulated and the correlation between them. The Fig. 4.7A shows the spatial statistical parametric maps on the group level with voxels significantly contributing with FC to each network ($p < 0.05$, FWE corrected at cluster level). Fig. 4.7B shows the average FC between networks averaged across participants, which were highly correlated and not significant different (range 0.42 - 0.6, $p > 0.05$, Bonferroni corrected). This means that each of the three target ROIs had strong baseline FC with its respective network and the three networks show equal functional connectivity among each other.

4.2.3 Regional analysis

To evaluate the local effect of TMS on the stimulated target areas, the fALFF and ReHo metrics were computed, reflecting both the amplitude of the low-frequency and the spatial coherence of the signal, respectively.

- **fALFF**: This metric did not show changes after TMS stimulation for either target-areas, neither the VIS target-area (mean pre = 0.24, SD = 0.19; mean post-VIS = 0.23, SD = 0.24; mean post-SAL = 0.27, SD = 0.22; mean post-Control = 0.27, SD = 0.24) nor the SAL target-area (mean pre = 0.70, SD = 0.19; mean post-VIS = 0.68, SD = 0.16; mean post-SAL = 0.67, SD = 0.27; mean post-Control = 0.71, SD = 0.22)

- **ReHo**: This metric did not show changes after TMS stimulation for either target-areas, neither the VIS target-area (mean pre = 0.66, SD = 0.42; mean

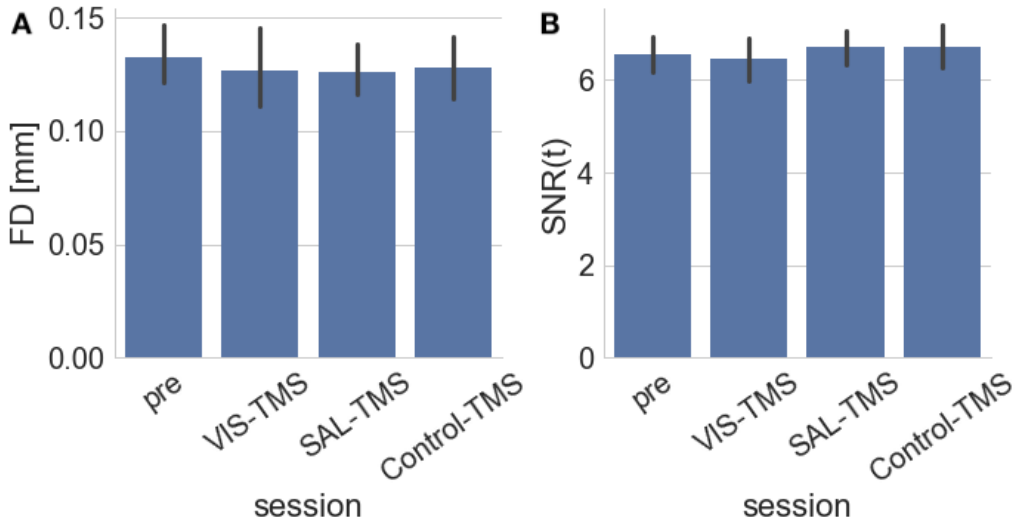

Fig. 4.6: Image quality assessment. There were not significant differences in the image QA metrics *(A)* framewise displacement (FD) and *(B)* temporal SNR (SNR(t)) across TMS sessions.

post-VIS = 0.57, SD = 0.45; mean post-SAL = 0.63, SD = 0.45; mean post-Control = 0.72, SD = 0.51) nor the SAL target-area (mean pre = 0.81, SD = 0.44; mean post-VIS = 0.94, SD = 0.31; mean post-SAL = 0.87, SD = 0.42; mean post-Control = 0.83, SD = 0.41)

Overall, TMS had no significant local effect on the stimulated target areas for either the fALFF or the ReHo metrics ($p > 0.05$, FWE corrected at cluster level. Fig. 4.8), showing a stable local amplitude of the low-frequency signal and spatial coherence after stimulation.

4.2.4 Network analysis

To evaluate the effect of TMS beyond the stimulation area, a voxel-wise FC analysis was carried out between the average time-series of the two stimulated iFC networks and the rest of the brain.

VIS stimulation

The stimulation of the VIS network, firstly, increased the brain FC. Secondly, this increase was observed in other brain networks, but not within the VIS network. Thirdly, all areas of increased FC were located in high-cognitive networks. Particularly, VIS-FC showed an increase in the FC of the posterior precuneus (PCUN) and

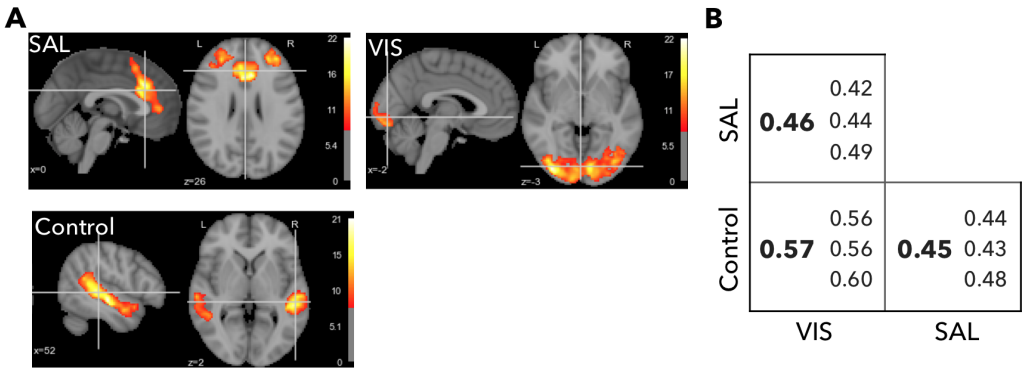

Fig. 4.7: Baseline functional connectivity. *(A)* Statistical parametric maps (p<0.05, FWE corrected at cluster level) of SAL, VIS, and STG (Control) networks averaged across all participants based on a FC analysis using individually defined TMS targets as seed areas. Color bars indicate z-score values. *(B)* Mean (BOLD) and session-specific Pearson correlation values between-network FC during pre-TMS averaged across all participants.

posterior cingulate gyrus (PCG), areas located within the DMN ($p < 0.001$, FWE corrected at cluster level), changes that are illustrated in the Fig. 4.9 (upper left) or extended in the Table 4.2 (VIS-FC). The SAL-FC showed an increase in the FC of the same areas with increased VIS-FC ($p = 0.003$, FWE corrected at cluster level), but also of both IPL, left anterior IPS, and the left middle frontal gyrus (middle frontal gyrus (MFG), $p < 0.001$, FWE corrected at cluster level). These changes are illustrated in the Fig. 4.9 (lower left) or extended in the Table 4.2 (SAL-FC).

In summary, VIS stimulation did not induce within-network effects, but instead, it increased the FC between both networks of interest, VIS and SAL, and the high-cognitive networks DMN, DAN, and CEN. The pie charts in Fig. 4.9 provides an extra assistance to visualize the distribution of the significantly affected voxels across the different brain iFC networks, which borders are overlaid on the cortical surface representations [Yeo et al., 2011].

SAL stimulation

The stimulation of the SAL network, firstly, decreased the brain FC, contrary to the effect observed after VIS stimulation. Secondly, it induced within-network effects, unlike VIS stimulation, which did not induce any. Thirdly, between network effects in areas located in high-cognitive networks were also observed. Finally, the SAL-FC showed a decrease in the FC of the left anterior insula (AI) and the dorsal anterior cingulate cortex (dACC), key nodes of the SAL network, but different from the stimulated target area. All changes are illustrated in the Fig. 4.9 (lower right) or

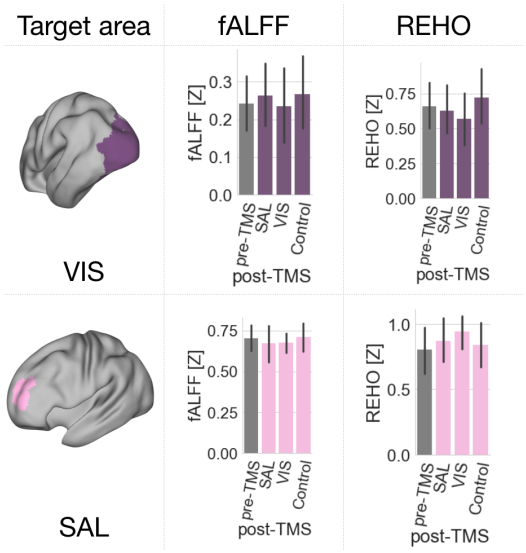

Fig. 4.8: No effect of TMS on local brain activity. (Left) From the fMRI BOLD-signal in the TMS target areas (VIS: top, SAL: bottom), two metrics reflecting local brain activity were computed, the fALFF (middle) and ReHo (right). Bar plots indicate the averaged metric value across all voxels of respective target areas, whereas error bars represent the 95% confidence interval of variance across participants.

extended in the Table 4.3 (SAL-FC) ($p < 0.0001$, FWE corrected at cluster level). On the other hand, the VIS-FC showed a decrease in the FC of both IPS, the middle temporal gyrus (MTG) and the left MFG ($p = 0.005$, FWE corrected at cluster level), changes that are illustrated in the Fig. 4.9 (upper right) or extended in the Table 4.3 (VIS-FC). In summary, SAL stimulation induced a decrease in the FC within the SAL network itself, but also between the VIS network and both attention networks, DAN, and CEN.

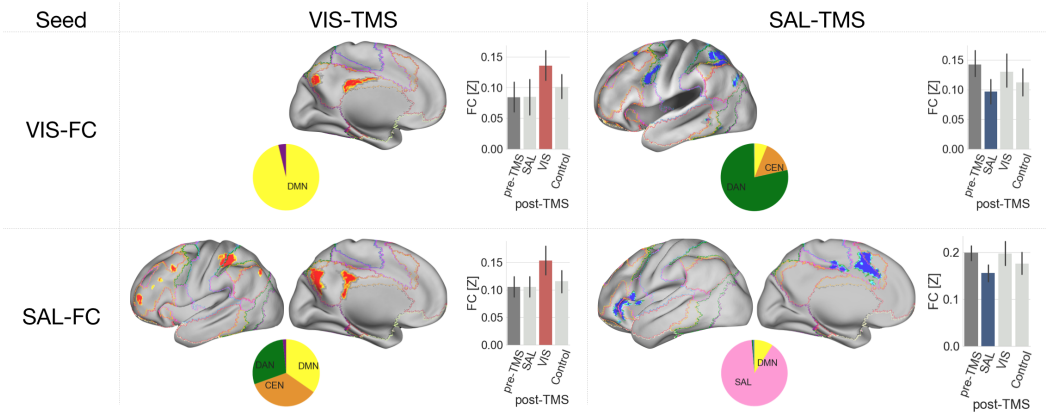

Fig. 4.9: Effect of TMS on brain network FC. Statistical parametric maps ($p < 0.01$, FWE corrected at cluster level) of changed FC are overlaid on the cortical surface of a standard brain. Bar plots illustrate average FC of significant voxels in each condition. Error bars indicate the 95% confidence interval of variance across subjects. Pie charts assign significant voxels to a standard set of functional brain networks [Yeo et al., 2011] illustrated with colored outlines on the cortical surface.

Overall, TMS had an opposite effect on the network brain FC. While VIS stimulation increased the FC, SAL stimulation decreased it. Nevertheless, only the SAL stimula-

Tab. 4.2: Brain regions where the VIS stimulation induced an increase in the network FC

VIS-FC									
Cluster			Peak			MNI	[mm]		Area
p(FWE)	p(unc)	k[vox]	p(FWE)	p(unc)	T	x	y	z	
0.000	0.000	242	0.158	0.000	5.16	8	-38	28	PCG
			0.954	0.000	4.21	-4	-38	28	
			0.962	0.000	4.19	-4	-24	28	
0.000	0.000	181	0.210	0.000	5.06	-10	-70	30	PCUN
			1.000	0.000	3.67	14	-60	32	
SAL-FC									
0.000	0.000	357	0.092	0.000	5.33	-10	68	18	FP
			0.270	0.000	4.96	-42	50	10	
			0.700	0.000	4.53	-24	64	16	
0.000	0.000	422	0.129	0.000	5.22	-6	-72	32	PCUN
			0.819	0.000	4.41	-18	-54	16	
			0.893	0.000	4.32	-12	-64	20	
0.001	0.000	145	0.209	0.000	5.05	-48	10	42	MFG
			0.999	0.000	3.92	-46	12	50	
0.001	0.000	139	0.231	0.000	5.02	48	-34	52	R IPL
0.000	0.000	494	0.237	0.000	5.01	-36	-38	44	L aIPS
			0.440	0.000	4.77	-42	-30	42	
			0.986	0.000	4.09	-44	-38	54	
0.003	0.000	115	0.688	0.000	4.54	-30	-80	40	L IPL
			0.985	0.000	4.10	-42	-72	38	
			1.000	0.000	3.66	-38	-80	36	
0.000	0.000	242	0.861	0.000	4.36	14	-60	32	PCUN
			0.947	0.000	4.22	8	-44	22	
			0.997	0.000	3.96	14	-54	24	
0.001	0.000	150	0.862	0.000	4.36	-30	18	34	MFG
			0.977	0.000	4.13	-46	22	32	
			0.999	0.000	3.92	-36	28	22	
0.000	0.000	269	0.927	0.000	4.26	38	-70	40	R IPL
			0.961	0.000	4.19	30	-72	40	
			0.977	0.000	4.13	24	-66	50	
0.000	0.000	163	0.929	0.000	4.26	-6	-44	14	pCG
			0.999	0.000	3.92	-6	-36	30	
			1.000	0.000	3.63	-6	-42	22	

tion induced within-network effects. Particularly, VIS stimulation increased the FC of the DMN and attention networks, DAN and CEN, whereas SAL stimulation decreased the FC within the SAL and between the VIS and attention networks. Finally, the Control stimulation had no significant changes in the network FC, increasing the specificity of these findings.

4.2.5 Brain graph modularity analysis

To further understand the effect of TMS on global functional integration, a graph-based consensus modularity analysis [Lancichinetti and Fortunato, 2012] was carried

Tab. 4.3: Brain regions where the SAL stimulation induced a decrease in the network FC

VIS-FC									
Cluster			Peak			MNI	[mm]		Area
p(FWE)	p(unc)	k[vox]	p(FWE)	p(unc)	T	x	y	z	
0.001	0.000	133	0.188	0.000	5.10	28	-60	36	R IPS
0.000	0.000	186	0.736	0.000	4.50	-46	-4	38	PreCG
			0.974	0.000	4.15	-46	4	30	
0.000	0.000	545	0.765	0.000	4.47	-30	-66	30	L IPS
			0.871	0.000	4.36	-34	-52	52	
			0.981	0.000	4.12	-34	-54	36	
0.000	0.000	155	0.853	0.000	4.38	-58	-48	-8	MTG
			0.991	0.000	4.06	-50	-58	-16	
			1.000	0.000	3.82	-50	-50	-4	
0.006	0.000	102	0.892	0.000	4.33	-20	14	50	SFG
			0.999	0.000	3.94	-26	8	50	
			1.000	0.000	3.82	-20	0	52	
0.005	0.000	104	0.958	0.000	4.20	-34	4	58	MFG
			0.994	0.000	4.03	-26	-8	62	
			1.000	0.000	3.52	-30	-4	52	
SAL-FC									
0.000	0.000	845	0.050	0.000	5.52	-50	12	-2	L AI
			0.100	0.000	5.30	-40	22	8	
			0.982	0.000	4.11	-32	4	8	
0.000	0.000	954	0.303	0.000	4.92	-10	6	50	dACC
			0.324	0.000	4.89	-2	16	28	
			0.462	0.000	4.75	-10	6	36	
0.000	0.000	227	0.925	0.000	4.27	14	-46	56	R SPL
			0.978	0.000	4.13	20	-50	52	
			0.999	0.000	3.92	16	-42	48	
0.007	0.000	102	0.999	0.000	3.89	-10	-24	38	L SPL
			1.000	0.000	3.85	-12	-14	38	

out in 77 nodes located in the brain networks found affected in the network analysis: VIS, SAL, DMN, DAN and CEN. This analysis allowed me to *(i)* derive a group level modular decomposition for every TMS session while preserving the inter-individual variability, and *(ii)* characterize the role of each node using topological analysis of the modular decomposition [Fornito et al., 2012; Dwyer et al., 2014].

Statistical significance

To test for the statistical significance of the modularity results, I checked that they were significantly more modular than expected by chance, ensuring that my findings are due to the TMS effect. This was examined at three different levels, at the level of each participant connectivity and co-classification matrices, and at the group level of each TMS-session co-classification matrix (Fig. 4.10). I found that the sample median Q across TMS sessions was significantly higher than expected by chance

when compared to the null model for the individual connectivity matrices (Q_{pre} = 0.181, Q_{VIS} = 0.143, Q_{SAL} = 0.165; $p < 0.001$), individual consistency matrices (Q_{pre} = 0.585, Q_{VIS} = 0.544, Q_{SAL} = 0.588; $p < 0.001$) and group consensus co-classification matrices (Q_{pre} = 0.266, Q_{VIS} = 0.244, Q_{SAL} = 0.274; $p < 0.001$). Overall, the modularity results were more modular than expected by chance at the three levels of randomization ($p < 0.001$), confirming that the findings observed on this section are due to the TMS effect and no to the chance.

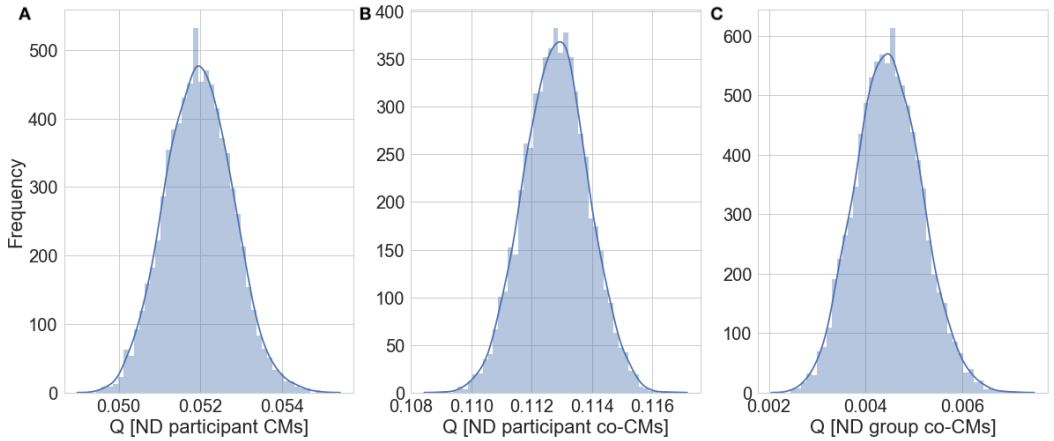

Fig. 4.10: Statistical significance of the modularity results. Null model distributions (ND) of median Q values based on the *(A)* individual functional connectivity matrices, *(B)* individual consistency matrices and *(C)* group consensus co-classification matrices. The modularity results were more modular than expected by chance at the three levels of randomization ($p < 0.001$).

Effect of TMS on the brain modular organization

To evaluate the effect of TMS on the modular brain function organization, the distribution of the nodes derived from the modularity analysis across all the identified modules was examined. I consistently found three main modules, which described the brain functional organization across all TMS sessions (Fig. 4.11), reflecting a stable network modularity (Q), which was not affected by the TMS effect ($p > 0.05$). The first module comprised mainly the VIS nodes (red module), the second one SAL nodes (green module) and the third one DMN nodes (blue module). The attention network nodes (CEN and DAN) were distributed across the three modules, but their module-affiliation was variable across TMS sessions. At baseline, the DAN nodes were distributed among the VIS and SAL modules (VIS: 57%, SAL: 43%), whereas the CEN nodes were distributed among the DMN and SAL modules (DMN: 57%, SAL: 43%; Fig. 4.11, left).

After stimulation, the attention network nodes changed their distribution across the modules. Particularly, VIS stimulation induced a change in the module-affiliation of most of the DAN and CEN nodes, moving them to the SAL module (86% of both networks nodes, Fig. 4.11 upper-right). On the other hand, SAL stimulation induced a change in the module-affiliation of all the DAN nodes for the SAL module, and of 15 % of the SAL nodes for the DMN module, including the stimulated target node, without affecting the overall distribution of CEN nodes between the DMN and SAL modules observed at baseline (Fig. 4.11 lower-right). Overall, TMS did not affect the modular brain function organization, observing three main modules dominating the functional organization across TMS sessions, nevertheless, the distribution of the attention networks nodes was altered differently after both TMS interventions.

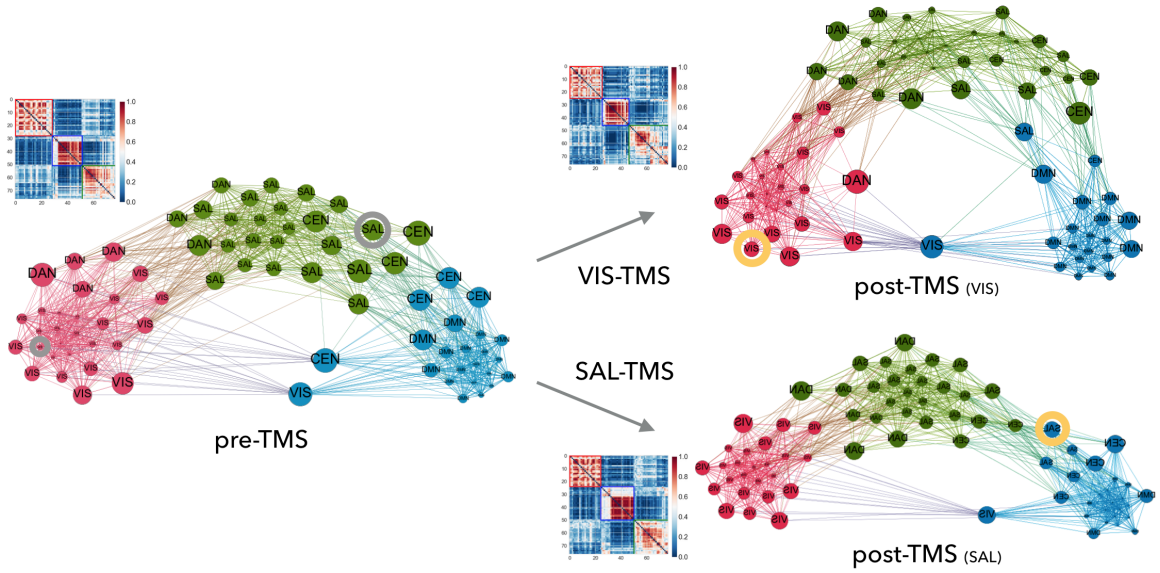

Fig. 4.11: Effect of TMS on the global brain network graph. Average co-classification matrices with their force-directed topological representations of the brain network graph calculated on pre- and post-TMS rs-fMRI data after VIS and SAL stimulation. In the topological representations, nodes with high co-classification values are located closer to each other, node color indicates the modular affiliation and node size represents the *h* value of each node. A high *h* value indicates strong interaction with other nodes in the whole graph, i.e. integration nodes. In each of the independently calculated co-classification matrices, the three modules cover mainly nodes of the VIS (red), DMN (blue) and SAL (green) networks with attention related nodes in between.

Local functional integration of the stimulated regions

To estimate the effect of TMS in the local functional integration of the stimulated regions, I examined the local node-degree, which provides information about the number of direct connections of a node. At the baseline condition, both target-nodes had a similar average node-degree, meaning that both of them interacted with the

same number of nodes across participants. Nonetheless, the VIS target-node was interacting mostly with nodes within its own module (node highlighted in gray in Fig. 4.12A left), whereas the SAL target-node was interacting with its own module, but also the DMN module (node highlighted in gray in Fig. 4.12B left).

After stimulation, both TMS interventions decreased the target-node-degree across participants (VIS: $p < 0.001$, Fig. 4.12A-middle; SAL: $p = 0.005$, Fig. 4.12B-middle), interacting less with other nodes across participants. Particularly, the VIS target-node shifted from the core to the periphery of its own module, interacting less with the core of the module (node highlighted in yellow in Fig. 4.12A right), whereas the SAL target-node shifted towards the DMN module, changing its module-affiliation and interacting less with the SAL module, which indicates that after SAL stimulation, it was more frequently co-classified within the DMN module across participants (node highlighted in yellow in Fig. 4.12B right).

To conclude, both VIS and SAL target regions had a similar node-degree at baseline, which decreased after stimulation, interacting less with the core of its baseline modules, moreover, the SAL target-node changed its module-affiliation to the DMN module, while continuing interacting with nodes from the SAL module.

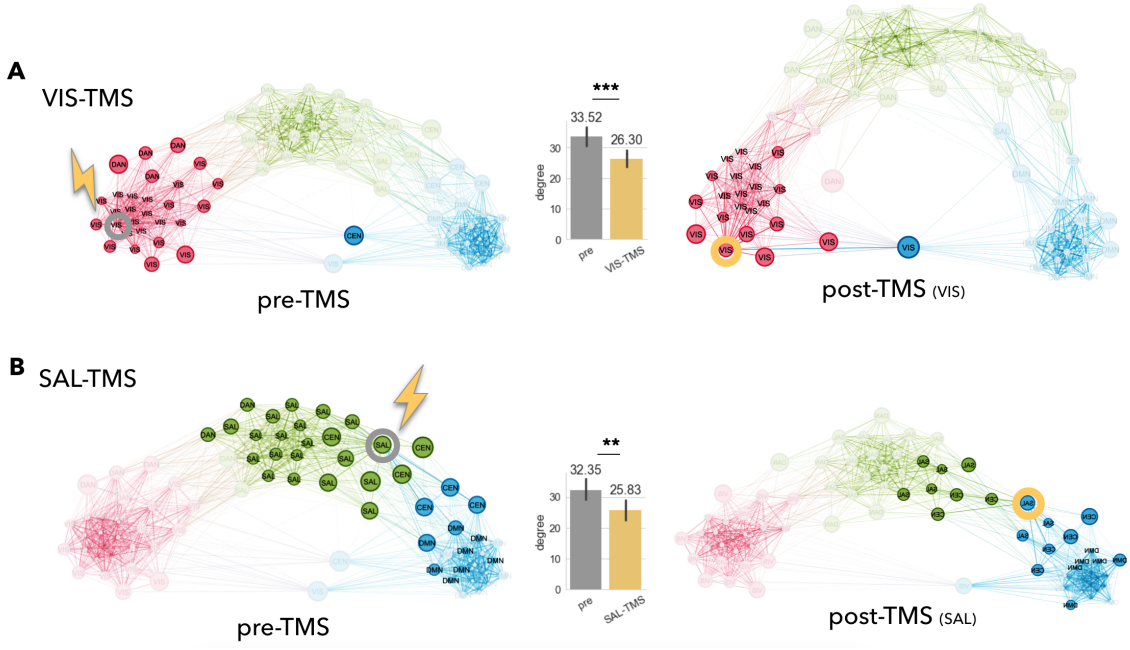

Fig. 4.12: Effect of TMS on the global interaction of the target nodes. TMS effect on degree of TMS targets. Same topological representation as in Fig. 4.11, yet highlighting only nodes with direct connections to the *(A)* VIS- and *(B)* SAL-TMS targets, before (grey circles) and after (yellow circles) stimulation. Bar plots illustrate consistently lower degree, i.e. average direct connections, of TMS target nodes after VIS-TMS and SAL-TMS.

Global brain functional integration

To estimate the functional integration of each module and their constituent nodes, I examined the consistency (z) and diversity (h) with which different regions were co-classified into the same module across participants, representing the functional integration within- and between-modules, respectively.

Starting with the local effect, VIS stimulation increased the target node's h (red highlighted nodes in Fig. 4.13 left; pre-h: 0.646, post-h: 0.882), whereas SAL stimulation did not affect it (green highlighted nodes in Fig. 4.13 right; pre-h: 0.919, post-h: 0.921). On the other hand, the Control stimulation increased slightly the target node's h (blue highlighted nodes in Fig. 4.13 middle; pre-h: 0.776, post-h: 0.863), compared to the VIS stimulation .

Similar to the local effects observed for h, but with an opposite direction, the target node's z decreased after all TMS interventions, conserving the same impact scale observed for the h, which was stronger after VIS stimulation (red highlighted nodes in Fig. 4.13A right; pre-z = 0.840, post-z = -0.228), compared to the Control stimulation (blue highlighted nodes in Fig. 4.13 middle; pre-z = 0.372, post-z = -0.242), as well as the SAL stimulation (green highlighted nodes in Fig. 4.13 middle; pre-z = -1.407, post-z = -1.879).

At the global level, consistently with the local effects, VIS stimulation increased the global brain's h (mean pre-h = 0.794, SD = 0.115; mean post-h = 0.83, SD = 0.07; p = 0.004; Fig. 4.13 left), whereas SAL stimulation did not induce any change on it (mean pre-h = 0.814, SD = 0.095; post-h = 0.808, SD = 0.1; $p > 0.05$; Fig. 4.13 right). Finally, Control stimulation increased slightly the global brain's h (mean pre-h = 0.819, SD = 0.081; mean post-h = 0.83, SD = 0.080; p = 0.02; Fig. 4.13 middle), compared to the VIS stimulation. In contrast, the global brain's z of the whole graph was not affected by either TMS intervention ($p > 0.05$, Fig. 4.13).

In summary, the between-module functional integration was affected differently depending on the stimulated areas, while VIS stimulation increased it locally and globally, SAL stimulation did not alter it. In addition, Control stimulation slightly increased it, locally and globally. On the other hand, the within-module functional integration was not altered by the TMS effect.

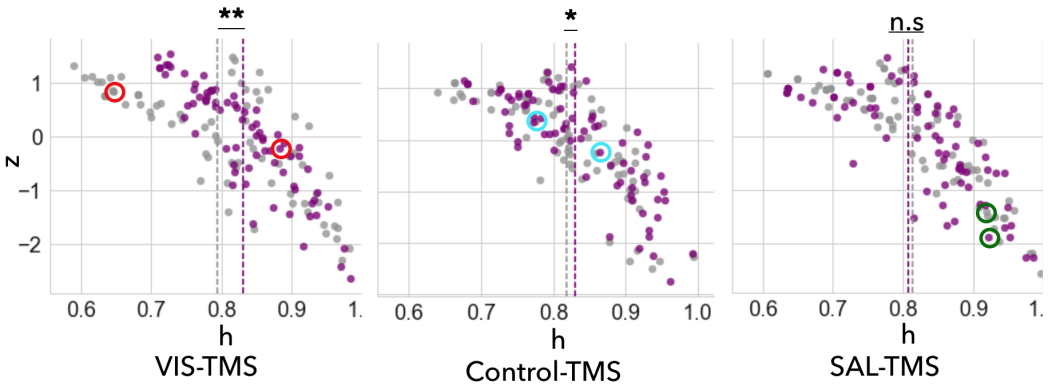

Fig. 4.13: TMS effect on global brain functional integration. Scatterplots of node distributions before (gray) and after (violet) TMS along axes of classification consistency *(z)* vs. classification diversity *(h)*. A higher *h* indicates stronger interaction with nodes of the whole graph, while a higher *z* indicates stronger interaction with nodes only of the same module. Average *h* of the whole graph increases after VIS-TMS (** p=0.004), but not after SAL-TMS (p>0.05). Average *z* is also not affected by either TMS intervention (p>0.05). In each scatterplot, circles highlight VIS (red) and SAL (green) TMS-targets before and after stimulation. Note that the increase of average h in the whole graph after VIS-TMS is associated with an increase in h of the TMS target node (pre-*h*: 0.65, post-*h*: 0.88).

Between-network brain functional integration

The previous results showed that *h* was sensitive to the effect of TMS depending on the stimulated area, showing a strong effect on the sensory network, VIS, a lighter effect on the control network, and no effect on the high-cognitive network SAL. Therefore, I inspected the distribution of this metric across the complete brain, which is illustrated in the Fig. 4.14, to further understand the differences between the three target areas, highlighted with circles in the same figure.

The spatial distribution of *h* across the brain shows that brain regions located in high-cognitive networks are more globally integrated (yellow), compared to areas located in sensory networks (blue). In particular, while the VIS target area is weakly integrated (red), the SAL target area is strongly integrated (green), whereas the control target area is located in a region with an intermediate global integration (cyan).

The results so far have been based on functional integration metrics derived from the modularity analysis. Hence, to support the graph based modularity findings, I estimated the within- and between-module node-degree based on the individual connectivity matrices of every participant at baseline. In line with the modularity analysis findings, the VIS module had an evidently higher within-module degree (mean = 12.22, SD = 5.66; $p < 0.001$), compared to the SAL (mean = 6.36, SD =

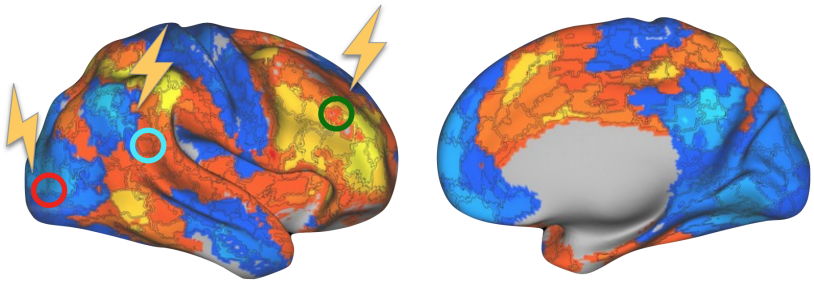

Fig. 4.14: Spatial distribution of h across the whole brain calculated on pre-TMS data showing lower h values (blue) in sensory and motor areas and higher h values in fronto-parietal areas (yellow), suggesting that TMS effects increase global interaction rather after stimulation of sensory-motor targets. The circles indicate the brain target areas stimulated in this study, VIS in red, SAL in green and Control in cyan.

4.78) and DMN (mean = 5.70, SD = 4.21) modules (Fig. 4.15A). In contrast, the difference was slighter when comparing the between-module degree across them, where only the DMN module had a significantly smaller between-module degree compared to the other modules (VIS: mean = 3.42, SD = 3.29; SAL: mean = 3.59, SD = 4.33; DMN: mean = 2.18, SD = 4.16, $p < 0.001$).

However, the interaction between the factors module and degree was significantly different. This is illustrated in Fig. 4.15B, where the ration between both degrees was plotted. The VIS module had a significantly higher ratio (mean = 5.38, SD = 4.72; $p < 0.001$), compared to the SAL (mean = 2.75, SD = 2.90) and DMN (mean = 3.24, SD = 3.75) modules. Moreover, this ratio was higher for the DMN module compared to the SAL module ($p = 0.045$). Consistent with the finding of the modularity analysis, the VIS module is predominantly internally connected, but weakly connected with other modules, whereas the SAL module has a higher interaction with other modules. In between, the DMN module had a similar degree ratio to the VIS module, being more internally connected and interacting less with other modules compared to the SAL module.

Combined with the findings from the Section 4.2.5, TMS of a weakly integrated brain network, here VIS, increased its local and global functional integration, whereas the stimulation of a highly integrated brain network, here SAL, had neither local nor global effects. Furthermore, this effect was not binary, and the Control stimulation has a lighter effect compared to VIS stimulation, increasing both the local and global functional integration (Fig. 4.13).

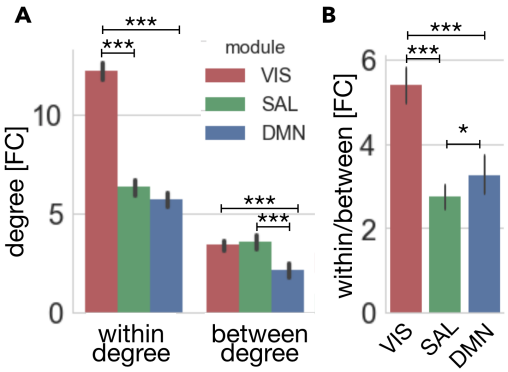

Fig. 4.15: Within- and between-module degree at baseline. *(A)* Bar plots illustrate the average within- and between-module degree (*x*-axis) for the VIS (red bars), SAL (green bars) and DMN (blue bars) modules. *(B)* Ratio between the within- and between-module degree, using the same color representation from (A). The within/between degree ratio was higher for the VIS module, compared to the DMN and SAL modules. In addition, the former module has a higher ratio than the latter one (* $p<0.05$, ** $p<0.01$, *** $p<0.001$).

5 Discussion

5.1 Project 1

In this study, which is already published [Preibisch & Castrillon et al. 2015], I evaluated four different mb-EPI protocols based on both the image quality assurance metrics (temporal SNR and structured noise) and the quality of the brain iFC networks derived from them, compared to the standard protocol. Altogether, the use of the minimum slice acceleration factor (M = 2) with an optimal combination of parameters, such as a reduced TR and a flip angle close to the Ernst angle, provided images with a data quality not significantly different to the reference protocol with a 2-fold in plane acceleration (SENSE). Hence, this led to an improvement in the temporal resolution of the fMRI acquisitions, which translated into better brain FC analysis or, alternatively, shortening of the acquisition time. However, higher slice acceleration factors (M>2) increasingly reduced the image quality, and thus, the sensitivity to detect brain iFC networks derived from those images.

5.1.1 The image quality decreases proportionally to the increase of the slice acceleration factor

The evaluation of different EPI protocols based only on the SNR is difficult, and it is even more difficult when they involved the use of multichannel coils [Dietrich et al., 2007; Triantafyllou et al., 2011], parallel imaging [Pruessmann et al., 1999; Preibisch et al., 2003; Breuer et al., 2009] and simultaneous multislice acquisitions [Xu et al., 2013]. Additionally, when they are used in the context of fMRI, the high contribution of physiological noise present in the signal complicates more this evaluation [Glover and Lai, 1998; Krüger and Glover, 2001; Triantafyllou et al., 2005; Triantafyllou et al., 2006; Triantafyllou et al., 2011]. To complement the information derived only from the SNR here, I evaluated the temporal SNR and apparent g-factor maps together, improving the assessment of the image quality for the specific case of fMRI. Compared to the reference EPI sequence (S2×M1) with a SENSE acceleration factor of 2 and no multiband acceleration (M = 1), the S2×M2 acquisition (M = 2, total acceleration factor 4), showed a minimal decrease in the temporal SNR, whereas the apparent g-factor map did not show a visible structured noise enhancement (Fig. 4.1).

With higher multiband acceleration factors (M > 2), both image quality metrics deteriorated, compared to the reference protocol. In particular, the protocol S2×M3 (M = 3, total acceleration factor 6) showed a significant reduction in temporal SNR of about 33% in several slices in some participants, a reduction that was evidenced as focal spots of noise enhancement visible in the spatial maps of temporal SNR (Fig. 4.1). Furthermore, the protocol S2×M4 (M = 4, total acceleration factor 8) had a strong reduction in the temporal SNR of about 64%, whereas the apparent g-factor maps showed a strong noise enhancement in areas located in the center of the images. These findings are in line with the previous work from Xu et al. [2013], who found a direct relationship between the g-factor and the multiband factor, where the g-factor increased by increasing the multiband factor. In addition, their g-factor histograms (Fig. 2 in Xu et al., 2013) show a high similarity to the ones presented here in Fig. 4.1C, considering that they reported the total acceleration factor, which is the multiplication of the slice- by the in-plane acceleration factor, meaning that is twice the M-factor reported here.

Finally, the temporal SNR of the truncated datasets was very similar to the ones derived from the the full datasets (Table 4.1, Fig. 4.2). This finding might be explained by the main contribution of physiological noise present in the fMRI signal of GM compared to WM areas [Krüger and Glover, 2001], which is in line with my results, where the SNR(t) was higher in WM, except for the S2×M4 images, where the artefacts in the center of the image decreased the overall temporal SNR in the WM (Table 4.1, Fig. 4.1).

5.1.2 Multiband increases the sensitivity of the FC analysis

The use of the multiband-EPI technique to acquire fMRI datasets improved the sensitivity of the FC analysis to detect brain iFC networks by increasing the slice factor to 3. In contrast, this sensitivity decreased with a slice factor of 4. The group FC analysis of the full datasets resulted in ten improved brain iFC networks, with greater spatial extent and higher peak values in their statistical maps (Fig. 4.3). This finding is consistent with previous studies from Feinberg et al. [2010] and Chen et al. [2015], who also observed an increase in the functional sensitivity at higher sampling acquisition rates.

Supported by the statistical analysis, the use of slice acceleration factors up to 3 increased the sensitivity of the FC analysis, improving the spatial extent and maximum Z-values of the brain iFC networks. On the other hand, for the slice acceleration factor of 4, the brain iFC networks presented image artefacts in almost all the networks, indicating that acceleration techniques enhance the structured

noise derived from residual unaliasing artefacts, which is prohibitive for functional imaging applications.

Similarly, the group FC analysis of the truncated datasets resulted in ten brain iFC networks homologous to the ones derived from the analysis of the full datasets. The statistical analysis showed that the use of a slice acceleration of 2 resulted in brain iFC networks that were not significantly different to those derived from the full dataset. On the other hand, the use of a slice acceleration of 3 reduced the sensitivity of the FC analysis, whereas the brain iFC networks derived from the dataset acquired with a slice acceleration factor of 4 significantly decreased their quality, reducing the spatial extent and peak Z-values across participants. Furthermore, the variability of spatial maps across participants was significantly affected (Fig. 4.3). These findings suggest that the use of short multiband-EPI acquisitions with higher temporal resolution is able to identify the most relevant brain iFC networks, with acquisition times down to 2.45 minutes (M = 3). While this analysis was restricted to rs-fMRI data, my data and also previous work of Feinberg et al. [2010] and Chen et al. [2015] suggest that sensitivity in task fMRI data will profit equally well from the implementation of multiband-EPI.

5.1.3 Conclusion

The results of this study show that multiband acceleration methods allow the simultaneous acquisition of multiple slices, nevertheless, it can affect the image quality and sensitivity in detecting brain iFC networks. In particular, the use of a multiband factor of 2 (combined with an in plane acceleration factor of 2, for total acceleration of 4) had a negligible SNR penalty, substantially improving the sensitivity in detecting brain iFC networks. In addition, the analysis of datasets acquired in half the time showed comparable results to the reference fMRI acquisition, providing an option to shorten the acquisition time in clinical studies. In contrast, the fMRI datasets acquired with a multiband factor of 4 (total acceleration of 8) were significantly degraded by structured noise enhancement, making them prohibitively for fMRI applications. Finally, the fMRI datasets acquired with a multiband factor of 3 (total acceleration of 6) improved the sensitivity in detecting brain iFC networks, although some focal noise enhancement was observed in the images of some participants, which might compromise the fMRI results overall.

To conclude, the use of multibanded fMRI acquisition using an acceleration factor of 2 had a minimal impact on the image quality and significantly increased the sensitivity and stability in detecting brain iFC networks, providing higher temporal resolution for research studies or shorten acquisition times for the clinical practice. Nevertheless, future improvements in the design and development of the acquisition

coils and in the reconstruction techniques used for multiband sequences could improve the image quality of fMRI datasets derived by using higher acceleration factors.

5.2 Project 2

In the present study, which is in preparation for publication at the submission date of this thesis, I assessed the effect of low-frequency rTMS in a sensory (left occipital pole in the VIS) and a high-cognitive (left DAPFC in the SAL) area on the brain functional connectivity at three different scales: regionally, within the stimulated region, network-wise, in remote brain regions interacting with the stimulated region, and globally, in the way the affected brain networks interacted with each other. In addition, I controlled for the specificity of the findings by contrasting them with the same results after stimulation of a control area, the superior temporal gyrus.

Overall, the results showed that TMS has different effects on both network and global functional integration depending on which cortical area was stimulated. The stimulation of a sensory input network, here VIS, led to specific increases in FC and functional integration of sensory and cognitive networks on a global level. The stimulation of a cognitive network, here SAL, led to widespread decreases in network FC, without changing global network integration. These findings suggest that low-frequency TMS is a useful tool for altering brain network communication beyond the stimulation spot, having stronger distant than local effects, and that spreading effects differ depending on whether sensory or high-cognitive brain regions are stimulated.

5.2.1 TMS did not alter the local brain activity of the stimulated regions

TMS has been successfully established to reliably modulate local brain activity and subsequent behavior in humans [Fox et al., 2012; Polania et al., 2018], primarily by stimulating superficial cortical neurons. However, TMS does not produce a focal stimulation of neuronal tissue at a small circumscribed site [Hartwigsen et al., 2009]. So far, the effects of TMS on the area of stimulation have been mainly studied in the primary motor cortex, where no local changes in the FC have been found, but rather an increase in remote areas [Bestmann and Feredoes, 2013]. The absence of local effects has been explained by Esser et al. [2005] using a modeling approach. The authors suggested that regional TMS effects are weak because both excitatory and inhibitory neural populations are affected, resulting in a low net effect that is difficult

to detect. Furthermore, it has been reported that local effects can be induced when suprathreshold TMS (MT > 100 %) is delivered to the cortex, reflecting the cortical processing of afferent input caused by the induced muscle contractions [Reithler et al., 2011].

In line with this argument, I did not observe local changes in the brain activity of the stimulated areas after TMS stimulation. Moreover, I extended previous results in two ways. First, I did not observe local effects using an rMT of 100%, extending the lack of local effects observed with subthreshold stimulation up to 100%. Second, the lack of local effects have been mostly observed in motor areas, while I here extend these findings to other sensory (VIS), and high-cognitive (SAL) areas. This finding is also supported by the fact that BOLD responses are more readily observed in remote regions due to the fact that the fMRI signal more closely reflects incoming and intracortical processing than spiking output [Logothetis, 2008; Logothetis et al., 2010; Reithler et al., 2011].

5.2.2 TMS induced area-dependent opposite brain changes

I found an opposite effect of inhibitory TMS on the network brain activity within the same participants, suggesting that the effect of the stimulation depends on the particular target area, and should not be generalized across the whole brain. The oversimplification of the term inhibitory TMS for interventions using low-frequency TMS was derived from studies stimulating motor areas [Kobayashi and Pascual-Leone, 2003; Hartwigsen et al., 2009; Polania et al., 2018], where a decrease of the motor evoked potential (MEP) has been interpreted as a cortical excitability decrease [Chen et al., 1997]. However, extrapolating this principle to other cortical areas does not seem to be straightforward, which is reflected in the heterogeneous findings reported in the literature using similar stimulation protocols, even for motor areas. Moreover, my results suggest that the effect of stimulation differs whether a brain region located in a sensory or a high-cognitive network is stimulated. Below I therefore discuss the results of this study differentiating between the effects on target areas located in sensory and high-cognitive networks.

TMS effect on sensory networks

I observed an increase in the FC of the sensory network VIS after stimulation. To my knowledge, only one study to date has combined inhibitory TMS with rs-fMRI to assess the effect of stimulation on the VIS network. Studying the relationship between the VIS and prefrontal areas, Cocchi et al. [2016] observed an increase in the FC after stimulation of the VIS network, which is consistent with the direction

of change induced by TMS observed here. In brain regions located in other sensory networks, inhibitory TMS has also induced an increase in the FC. In the SM network, Watanabe et al. [2014] examined the effect of stimulation on the left M1, finding an increase the FC. In the contralateral brain area, Cocchi et al. [2015] assessed the changes in the brain integration, observing an increase in the within-module FC, but a decrease in the between-module FC.

In contrast, some studies have observed a decrease in the FC after stimulation of brain regions located in the SM network with inhibitory TMS. In particular, Valchev et al. [2015] tested the possibility of modulating S1 without conducting a task, observing a decrease on the contralateral PMd. Stimulating another somatosensory area, Watanabe et al. [2015] derived causal information from the relationship between the pre-SMA and deep brain structures by inhibiting the pre-SMA, observing a decrease in the FC.

Overall, inhibitory TMS seems to increase the FC after stimulation of the VIS network. In addition, this finding seems to be applicable to other sensory areas, particularly, the M1 in the SM network, where previous studies have observed an increase in the FC as well. However, this effect cannot be generalized to all sensory networks, where previous studies have observed a decrease rather than an increase in the FC after stimulation of S1 in the SM network.

TMS effect on high-cognitive networks

I observed a decrease in the FC of the high-cognitive network SAL after stimulation. To my knowledge, no study so far has combined inhibitory TMS with rs-fMRI to assess the effect of stimulation on the prefrontal region of the SAL network. Nevertheless, the prefrontal cortex is involved in multiple brain networks [Power et al., 2011; Yeo et al., 2011; Yeo et al., 2014], and thus, several studies have assessed the effect of stimulation in the context of other brain networks [Werf et al., 2010; Chen et al., 2013; Mastropasqua et al., 2014; Cocchi et al., 2016]. Specifically, two studies evaluating the effect of stimulation in prefrontal areas located in the attention networks support my findings, observing a decrease in the FC. Mastropasqua et al. [2014] evaluated the effect of inhibitory TMS on the right DLPFC, within the CEN, observing a decrease in the FC of the same network. Moreover, Cocchi et al. [2016] tested the relationship between prefrontal areas of the DAN and the VIS network by stimulating the right FEF, observing a decrease in the FC of the VIS network.

In addition to the studies evaluating the TMS effects on prefrontal areas within attention networks, the relationship of prefrontal areas with the DMN has been also

evaluated. However, the results of these studies are heterogeneous. Supporting my findings, Van der Werf et al. [2010] evaluated the effect of stimulating the left DLPFC in different brain networks, reporting a decrease in the FC of both temporal lobes and hippocampal areas. On the other hand, results that contradict mine have been also observed. Chen et al. [2013] evaluated the relationship between prefrontal areas located in the CEN and SAL with the DMN, observing a shift of DMN signal from its low-frequency range to a higher frequency, suggesting an increase of the DMN activity.

Despite the heterogeneous results in the DMN, previous studies stimulating prefrontal areas located within the attention networks CEN and DAN support the findings observed here in the SAL network, decreasing the FC within the network or with other positively correlated networks. Something these networks have in common is the positive correlation between them at rest [Fox and Raichle, 2007; Power et al., 2011; Yeo et al., 2014; Glasser et al., 2016], suggesting that the expected effect of inhibitory TMS on a remote brain region could be constrained by the relationship between the remote and the target region at rest. Supporting this argument, Chen et al. [2013] explicitly tested the negative relationship between the SAL and CEN with the DMN, observing an increase in the FC of the latter network after inhibitory TMS of the former ones.

Nevertheless, brain function is complex, and even within the same network, it is possible to find subsystems with different relationships between them. For example, Van der Werf et al. [2010] observed that inhibitory TMS induced a decrease in the FC of hippocampal areas, regions that have been previously found to be negatively correlated with other areas within the DMN, such as the IPL [Fox et al., 2005; Fox et al., 2012]. In line with those results, Eldaief et al. [2011] observed an increase in the FC of hippocampal areas after stimulating the IPL with inhibitory TMS.

Overall, inhibitory TMS on high-cognitive networks seems to affect the FC within the stimulated network and functionally correlated networks. However, the effect induced depends on the target area, and its relationship with the network evaluated at rest. While inhibitory TMS decrease the FC of positively correlated areas, it increases it among negatively correlated ones, which is consistent with the functional relationship between them at rest. Moreover, the same principle seems to apply to subsystems within a particular brain network. Altogether, here I found a differential effect of TMS depending on whether a sensory, here VIS, or a high-cognitive network, here SAL, were inhibited with TMS. While the FC increased after VIS stimulation, it decreased after SAL stimulation.

5.2.3 TMS induced brain changes with a network-dependent extent

I found within-network effects after SAL stimulation. Specifically, inhibitory TMS decreased the FC of left AI and dACC, core components of the SAL network, which have been systematically observed to be functionally connected and share structural architecture at the cellular level [Uddin, 2015; Menon, 2015]. Furthermore, the stimulated target area was not affected by the TMS effect, which is consistent with the results at the regional level. Compared to previous studies, to my knowledge, only Gratton et al. [2013] have studied the effect of inhibitory TMS on the SAL but stimulating a different area, the left AI. Nonetheless, contrary to my results, they did not find within-networks effects. Finally, previous studies stimulating other high-cognitive networks have also observed within-network effects on the DMN [Eldaief et al., 2011] and CEN [Mastropasqua et al., 2014].

In contrast to SAL stimulation, I did not observe within-network changes after VIS stimulation. This finding contradicts the results of previous studies stimulating areas in the VIS network with inhibitory TMS, which induced within-networks changes [Rahnev et al., 2013; Cocchi et al., 2016]. This difference could be explained by the use of different experimental procedures or the different state of the participants during the stimulation; participants had their eyes closed when stimulated, whereas I stimulated participants who had their eyes open. This difference in the state of the participants during stimulation has been observed to be an important factor in the behavioral after effect of stimulation, having a higher effect on the low active neural state, like the eyes closed [Silvanto et al., 2007; Rahnev et al., 2013]. Finally, previous studies stimulating other sensory networks have also observed within-network effects on the SM network [Watanabe et al., 2014; Watanabe et al., 2015; Cocchi et al., 2015].

In addition to the within-network changes, I observed between-network changes after both SAL and VIS stimulation. In particular, SAL stimulation altered the interaction between the VIS and DAN, networks hierarchically correlated [Yeo et al., 2011; Spadone et al., 2015]. This decrease in the interaction between these networks could have been driven by the within-network changes observed on the left AI, an important brain hub with a switching role between brain networks, including the SAL and DAN [Uddin, 2015; Menon, 2015]. Moreover, the target area for the SAL stimulation has been previously reported to be an association area between dorsal and ventral attention networks [Asplund et al., 2010; Yeo et al., 2011; Yeo et al., 2014], supporting the changes induced in the interaction between them. Similarly, Gratton et al. [2013] observed between-network changes after disruption of the SAL. Even though they affected areas in different networks, CEN and DMN, they

are in line with my results, evidencing the role of SAL in the dynamic switching between networks [Bressler and Menon, 2010; Menon, 2015]. The difference in the observed affected networks might be explained by the stimulation of a different area, the AI.

On the other hand, VIS stimulation only induced between-network effects. Specifically, it seems to strongly affect DAN related areas, a network involved in the hierarchical visual system and highly correlated with the VIS [Gilbert and Li, 2013; Spadone et al., 2015]. This hierarchical relationship between VIS and DAN has been previously assessed in combined TMS-fMRI studies, where the stimulation of VIS has altered both networks [Ruff et al., 2006; Heinen et al., 2014; Cocchi et al., 2016]. Evaluating this interaction with inhibitory TMS and rs-fMRI, Cocchi et al. [2016] observed between-network effects in precuneus and DAN areas, which were found to be affected by the VIS stimulation in my network analysis results (Section 4.2.4), suggesting that the modulation of DAN with VIS stimulation is a strong and reproducible effect.

Furthermore, I found that VIS stimulation increased the FC between the VIS and DMN, specifically the posterior cingulate cortex and precuneus, areas associated with the recruitment of visual attention during episodic retrieval [Nelson et al., 2010; Power et al., 2011; Guerin et al., 2012] and negatively correlated with the DAN [Fox et al., 2005; Murphy et al., 2009; Anderson et al., 2011]. This finding suggests that the stimulation of the VIS can affect areas involved in memory functions, a relationship that has been explored previously by the study of the contribution of the sensory cortex to memory functions [Ven and Sack, 2013]. However, behavioral measures would be needed to confirm this interpretation.

Finally, I observed that VIS stimulation induced an increase in the FC between the SAL and both attention networks, DAN and CEN. In conjunction with the previous between-network findings, VIS stimulation seems to alter not just a single network but all the networks involved in the visual processing. This effect of NIBS on VIS areas has been previously studied, where a transient interference with perception has been observed [Bestmann and Feredoes, 2013; Amassian et al., 1989; Amassian et al., 1993; Maccabee et al., 1991]. Nevertheless, it would be necessary to add behavioral measures to test this interpretation.

Overall, the stimulation of both brain networks led to widespread changes in the FC, mainly in areas located within the attention networks. However, only SAL stimulation induced changes within the same network, whereas VIS stimulation only affected high-cognitive networks, including the DMN. Altogether, TMS seems to have stronger distant than local effects, having a widespread effect on brain function,

areas that might be related with the networks involved in the visual processing system.

5.2.4 TMS altered selectively the brain global integration

Brain function has been observed to have a modular organization, supporting localized specialization of brain functions within modules, which are highly integrated within themselves but weakly connected with other modules. While sensory functions support this localized specialization, high-cognitive functions are usually not localized within one module, instead, they involve the interaction between different ones [Bullmore and Sporns, 2012; Bassett et al., 2013; Braun et al., 2015; Rubinov, 2015; Fornito et al., 2016; Sporns and Betzel, 2016]. Here, I observed a highly modular brain structure, higher than could have been expected to occur by chance, consistent across all TMS conditions, and represented by three modules resembling the VIS, SAL and DMN modules, whereas the attention network nodes were distributed across the modules. The distribution of the attention network nodes across the modules is consistent with the integrative role of these networks, which integrate and coordinate the connectivity between different modules, keeping the global brain modular structure by frequently changing their module-affiliation as a function of the performed task [Bassett et al., 2013; Yeo et al., 2014; Bertolero et al., 2015].

Even though the distribution of the core nodes of every module was relatively stable across the sessions, TMS induced *(i)* a local decrease in the functional communication of the target nodes with the core of their modules, reflected in the decrease of the nodal degree, and *(ii)* a reconfiguration on the distribution of the attention network nodes and the SAL nodes with a high interaction with the DMN module across TMS sessions. This suggests that TMS alters the brain integration within and between the different modules. Therefore, the characterization of the interaction between the modules and their constituent nodes through the diversity classification parameter provided me with a better understanding of the between-networks changes induced by inhibitory TMS, where a change in brain integration can be interpreted as a reconfiguration of the interaction between the modules.

The stimulation of the weakly integrated VIS target node increased both, the nodal and global brain integration, whereas the stimulation of the highly integrated SAL target node did not affect the brain integration. Besides the striking difference in effect depending on the stimulated area and the induced increase of the local integration on the VIS target node, the local effect seems to spread to the whole brain, which is reflected in the overall increase of the classification diversity. To my knowledge, the effect of focal perturbations on global functional integration

across the cortex has never been tested experimentally, but only hypothesized by computational modeling methods [Muldoon et al., 2016; Gollo et al., 2017].

Muldon et al. [2016] evaluated the impact of focal perturbations on brain network activity by using network control theory [Gu et al., 2015]. The authors observed that the disturbance of brain regions with a high nodal-strength within the same module, such as the sensory and DMN networks [Power et al., 2011], produced a high spreading change. The disturbance of brain regions with lower nodal-strength, such as some SAL areas, only produced smaller effects due to the sparsity of their connected areas. Similarly, Gollo et al. [2017] evaluated the impact of focal perturbations on brain network activity by using a computational model of synchronization, the Kuramoto model [Kuramoto, 1984]. They observed that local stimulation is more likely to change the patterns of connectivity of brain regions within a peripheral system, such as the sensory network, than of areas in a high-level system, such as the SAL.

My experimental results were consistent with the results of both computational modeling studies. Firstly, I found that the stimulation of the sensory network VIS induced a widespread increase in global brain integration. While Muldoon et al. [2016] attributed this effect to functionally densely connected areas located within sensory and DMN networks, Gollo et al. [2017] attributed it to more peripherally located regions, which are weakly connected and have flexible dynamics. Secondly, I observed that the stimulation of the high-cognitive network SAL did not induce any effect. Muldoon et al. [2016] attributed this effect to the difficulty of controlling sparsely connected areas, such as the prefrontal area, whereas Gollo et al. [2017] attributed it to the more stable and constrained dynamics of core regions, e.g. high-cognitive networks. Finally, Gollo et al. [2017] predicted an increase in the FC of peripheral regions such as VIS after inhibitory stimulation, and a decrease of core areas as SAL. Both predicted changes are in line with my results, where I observed an increase in the FC and brain integration after VIS stimulation and a decrease of the brain FC after SAL stimulation.

In summary, the stimulation of a within-module node such as VIS induced an increase of nodal brain integration, spreading to the rest of the brain and affecting the overall global brain integration. On the other hand, the stimulation of a highly-globally connected network such as SAL did not affect the global brain integration.

5.2.5 Conclusion

It has been shown that TMS modulates neural activity far beyond the site of stimulation, having a distributed effect on brain function. However, the spread of the

TMS-effects and the analysis of these effects in early sensory and higher cognitive brain networks have not been systematically studied yet. Here, I compared three different TMS-sites in healthy participants, observing that TMS has a differential effect depending on whether an early sensory or a higher cognitive brain network was stimulated regarding *(i)* the direction of the change (Section 5.2.2), *(ii)* the spatial extent of these changes (Section 5.2.3) and *(iii)* global brain functional integration (Section 5.2.4).

Although previous studies have observed similar findings when either the same network or the same type of network was stimulated, those results are highly heterogeneous, and no study so far has characterized the effects of inhibitory TMS in both types of networks. Therefore, I presented a within-subject design where both types of networks were stimulated. In addition, the effects were contrasted with an active control session. In principle, TMS had a clear opposite effect on brain FC, increasing after VIS stimulation but decreasing after SAL stimulation. However, while SAL stimulation effects were localized in core areas of the SAL network and highly correlated networks, VIS stimulation affected areas were spread across different high-cognitive networks.

Therefore, to further understand the observed spread effects of TMS, especially after VIS stimulation, I characterized the global integration of the brain networks found affected in the network FC analysis. I found a strong increase in local brain integration, which was spread through all networks after VIS stimulation, but not after SAL stimulation. This global increase of functional integration was consistent with previous studies that have used computational modeling methods to predict the effect of an external focal perturbation on global brain activity [Cocchi et al., 2016; Muldoon et al., 2016; Gollo et al., 2017]. Particularly, I experimentally confirmed the modeling predictions derived from these studies for areas located in sensory and high-cognitive networks.

To conclude, my results strongly suggest that TMS would appear to have stronger distant than local effects and the type and spread of these effects differ depending on whether a sensory or a cognitive brain region is stimulated. Nevertheless, the addition of behavioral tests related to the brain processes found to be affected by TMS in this thesis, such as visual perception or memory, or the use of computational modelling methods would be recommended in order to validate my results.

References

Allen, Elena A., Erik B. Erhardt, Eswar Damaraju, et al. (2011). „A Baseline for the Multivariate Comparison of Resting-State Networks“. In: *Front. Syst. Neurosci.*

Amassian, V. E., Roger Q Cracco, P. J. Maccabee, et al. (1989). „Suppression of visual perception by magnetic coil stimulation of human occipital cortex.“ In: *Electroencephalography and clinical neurophysiology* 74 6, pp. 458–62.

Amassian, V. E., P. J. Maccabee, Roger Q Cracco, et al. (1993). „Measurement of information processing delays in human visual cortex with repetitive magnetic coil stimulation.“ In: *Brain research* 605 2, pp. 317–21.

Anderson, Jeffrey S., T. Jason Druzgal, Melissa Lopez-Larson, et al. (2011). „Network anticorrelations, global regression, and phase-shifted soft tissue correction.“ In: *Human brain mapping* 32 6, pp. 919–34.

Andoh, J., R. Matsushita, and R. J. Zatorre (2015). „Asymmetric Interhemispheric Transfer in the Auditory Network: Evidence from TMS, Resting-State fMRI, and Diffusion Imaging“. In: *Journal of Neuroscience*.

Asplund, Christopher L., Jay Todd, A. P. Snyder, and René Marois (2010). „A central role for the lateral prefrontal cortex in goal-directed and stimulus-driven attention“. In: *Nature Neuroscience*.

Awiszus, Friedemann (2003). „TMS and threshold hunting“. In: *Supplements to Clinical neurophysiology*. Vol. 56. Elsevier, pp. 13–23.

Bassett, Danielle S., Nicholas F. Wymbs, M. Puck Rombach, et al. (2013). „Task-Based Core-Periphery Organization of Human Brain Dynamics“. In: *PLoS Computational Biology*.

Beckmann, Christian F. and Stephen M. Smith (2004). „Probabilistic independent component analysis for functional magnetic resonance imaging“. In: *IEEE Transactions on Medical Imaging* 23, pp. 137–152.

Beckmann, Christian F, Clare E Mackay, Nicola Filippini, and Stephen M Smith (2009). „Group comparison of resting-state FMRI data using multi-subject ICA and dual regression“. In: *Neuroimage* 47.Suppl 1, S148.

Behzadi, Yashar, Khaled Restom, Joy Liau, and Thomas T. Liu (2007). „A component based noise correction method (CompCor) for BOLD and perfusion based fMRI“. In: *NeuroImage* 37 1, pp. 90–101.

Bertolero, Maxwell A., B. T. Thomas Yeo, and Mark D'Esposito (2015). „The modular and integrative functional architecture of the human brain." In: *Proceedings of the National Academy of Sciences of the United States of America* 112 49, E6798–807.

Bestmann, Sven and Eva Feredoes (2013). „Combined neurostimulation and neuroimaging in cognitive neuroscience: Past, present, and future". In: *Annals of the New York Academy of Sciences*.

Bestmann, Sven, Jürgen Baudewig, Hartwig R. Siebner, John C. Rothwell, and Jens Frahm (2005). „BOLD MRI responses to repetitive TMS over human dorsal premotor cortex". In: *NeuroImage*.

Bilek, E., A. Schafer, E. Ochs, et al. (2013). „Application of High-Frequency Repetitive Transcranial Magnetic Stimulation to the DLPFC Alters Human Prefrontal-Hippocampal Functional Interaction". In: *Journal of Neuroscience*.

Blondel, Vincent D, Jean-Loup Guillaume, Renaud Lambiotte, and Etienne Lefebvre (2008). „Fast unfolding of communities in large networks". In: *Journal of statistical mechanics: theory and experiment* 2008.10, P10008.

Braun, Urs, Axel Schäfer, Henrik Walter, et al. (2015). „Dynamic reconfiguration of frontal brain networks during executive cognition in humans." In: *Proceedings of the National Academy of Sciences of the United States of America* 112 37, pp. 11678–83.

Bressler, Steven L. and Vinod Menon (2010). „Large-scale brain networks in cognition: emerging methods and principles". In: *Trends in Cognitive Sciences* 14.6, pp. 277–290.

Breuer, Felix, Martin Blaimer, Robin M. Heidemann, et al. (2005). „Controlled aliasing in parallel imaging results in higher acceleration (CAIPIRINHA) for multi-slice imaging." In: *Magnetic resonance in medicine* 53 3, pp. 684–91.

Breuer, Felix, Stephan A. R. Kannengiesser, Martin Blaimer, et al. (2009). „General formulation for quantitative G-factor calculation in GRAPPA reconstructions." In: *Magnetic resonance in medicine* 62 3, pp. 739–46.

Bullmore, Ed. and Olaf Sporns (2012). „The economy of brain network organization". In: *Nature Reviews Neuroscience* 13, pp. 336–349.

Chen, Ashley C., Desmond J. Oathes, Catie Chang, et al. (2013). „Causal interactions between fronto-parietal central executive and default-mode networks in humans." In: *Proceedings of the National Academy of Sciences of the United States of America* 110 49, pp. 19944–9.

Chen, L., An T. Vu, Junqian Xu, et al. (2015). „Evaluation of highly accelerated simultaneous multi-slice EPI for fMRI". In: *NeuroImage* 104, pp. 452–9.

Chen, RMMF, Joseph Classen, Christian Gerloff, et al. (1997). „Depression of motor cortex excitability by low-frequency transcranial magnetic stimulation". In: *Neurology* 48.5, pp. 1398–1403.

Cocchi, Luca, Martin V. Sale, Anton Lord, et al. (2015). „Dissociable effects of local inhibitory and excitatory theta-burst stimulation on large-scale brain dynamics". In: *Journal of Neurophysiology*.

Cocchi, Luca, Martin V. Sale, Leonardo L. Gollo, et al. (2016). „A hierarchy of timescales explains distinct effects of local inhibition of primary visual cortex and frontal eye fields". In: *eLife*.

Craddock, Cameron, Sharad Sikka, Brian Cheung, et al. (2013). „Towards automated analysis of connectomes: The configurable pipeline for the analysis of connectomes (c-pac)“. In: *Front Neuroinform* 42.

Dietrich, Olaf, José Raya, Scott. B Reeder, Maximilian Reiser, and Stefan O. Schoenberg (2007). „Measurement of signal-to-noise ratios in MR images: influence of multichannel coils, parallel imaging, and reconstruction filters.“ In: *Journal of magnetic resonance imaging : JMRI* 26 2, pp. 375–85.

Dwyer, D. B., B. J. Harrison, M. Yucel, et al. (2014). „Large-Scale Brain Network Dynamics Supporting Adolescent Cognitive Control“. In: *Journal of Neuroscience*.

Eldaief, M. C., M. A. Halko, R. L. Buckner, and A. Pascual-Leone (2011). „Transcranial magnetic stimulation modulates the brain's intrinsic activity in a frequency-dependent manner“. In: *Proceedings of the National Academy of Sciences*.

Esser, Steve K., Sean L. Hill, and Giulio Tononi (2005). „Modeling the effects of transcranial magnetic stimulation on cortical circuits.“ In: *Journal of neurophysiology* 94 1, pp. 622–39.

Feinberg, David A. and Kawin Setsompop (2013). „Ultra-fast MRI of the human brain with simultaneous multi-slice imaging.“ In: *Journal of magnetic resonance* 229, pp. 90–100.

Feinberg, David A., Steen Moeller, Stephen M. Smith, et al. (2010). „Multiplexed Echo Planar Imaging for Sub-Second Whole Brain FMRI and Fast Diffusion Imaging“. In: *PloS one*.

Filippini, Nicola, Bradley J. MacIntosh, Morgan G. Hough, et al. (2009). „Distinct patterns of brain activity in young carriers of the APOE-epsilon4 allele.“ In: *Proceedings of the National Academy of Sciences of the United States of America* 106 17, pp. 7209–14.

Fornito, A., B. J. Harrison, A. Zalesky, and J. S. Simons (2012). „Competitive and cooperative dynamics of large-scale brain functional networks supporting recollection“. In: *Proceedings of the National Academy of Sciences*.

Fornito, Alex, Andrew Zalesky, and Edward Bullmore (2016). *Fundamentals of brain network analysis*. Academic Press.

Fox, Michael D and Marcus E Raichle (2007). „Spontaneous fluctuations in brain activity observed with functional magnetic resonance imaging“. In: 8.September.

Fox, Michael D., Abraham Z. Snyder, Justin L. Vincent, et al. (2005). „The human brain is intrinsically organized into dynamic, anticorrelated functional networks.“ In: *Proceedings of the National Academy of Sciences of the United States of America* 102 27, pp. 9673–8.

Fox, Michael D, Abraham Z Snyder, Jeffrey M Zacks, and Marcus E Raichle (2006). „Coherent spontaneous activity accounts for trial-to-trial variability in human evoked brain responses“. In: *Nature neuroscience* 9.1, p. 23.

Fox, Michael D., Mark A. Halko, Mark C. Eldaief, and Alvaro Pascual-Leone (2012). *Measuring and manipulating brain connectivity with resting state functional connectivity magnetic resonance imaging (fcMRI) and transcranial magnetic stimulation (TMS)*.

Friston, KJ, CD Frith, PF Liddle, and RSJ Frackowiak (1993). „Functional connectivity: the principal-component analysis of large (PET) data sets“. In: *Journal of Cerebral Blood Flow & Metabolism* 13.1, pp. 5–14.

Gilbert, Charles D. and Wu Li (2013). „Top-down influences on visual processing“. In: *Nature Reviews Neuroscience* 14, pp. 350–363.

Glasser, Matthew F., Timothy S. Coalson, Emma C. Robinson, et al. (2016). „A multi-modal parcellation of human cerebral cortex“. In: *Nature* 536.7615, pp. 171–178.

Glover, G. H. and Samuel K Lai (1998). „Self-navigated spiral fMRI: interleaved versus single-shot.“ In: *Magnetic resonance in medicine* 39 3, pp. 361–8.

Gollo, Leonardo L., James A. Roberts, and Luca Cocchi (2017). „Mapping how local perturbations influence systems-level brain dynamics“. In: *NeuroImage*.

Good, Benjamin H., Yves-Alexandre de Montjoye, and Aaron Clauset (2010). „Performance of modularity maximization in practical contexts.“ In: *Physical review. E, Statistical, nonlinear, and soft matter physics* 81 4 Pt 2, p. 046106.

Gratton, Caterina, Taraz G. Lee, Emi M. Nomura, and Mark D'Esposito (2013). „The effect of theta-burst TMS on cognitive control networks measured with resting state fMRI“. In: *Frontiers in Systems Neuroscience*.

Gu, Shi, Fabio Pasqualetti, Matthew Cieslak, et al. (2015). „Controllability of structural brain networks“. In: *Nature communications*.

Guerin, Scott A., Clifford A. Robbins, Adrian W. Gilmore, and Daniel L. Schacter (2012). „Interactions between Visual Attention and Episodic Retrieval: Dissociable Contributions of Parietal Regions during Gist-Based False Recognition“. In: *Neuron* 75, pp. 1122–1134.

Hallett, Mark (2007). *Transcranial Magnetic Stimulation: A Primer*.

Hartwigsen, Gesa, Tanja Kassuba, and Hartwig R. Siebner (2009). „Combining Transcranial Magnetic Stimulation with (f)MRI“. In:

Heinen, Klaartje, Eva Feredoes, Nikolaus Weiskopf, Christian C. Ruff, and Jon Driver (2014). „Direct evidence for attention-dependent influences of the frontal eye-fields on feature-responsive visual cortex“. In: *Cerebral Cortex*.

Heuvel, Martijn P. van den and Hilleke E. Hulshoff Pol (2010). „Exploring the brain network: A review on resting-state fMRI functional connectivity“. In: *European Neuropsychopharmacology* 20.8, pp. 519–534.

Huber, Reto, Steve K. Esser, Fabio Ferrarelli, et al. (2007). „TMS-Induced Cortical Potentiation during Wakefulness Locally Increases Slow Wave Activity during Sleep“. In: *PLoS ONE* 2, pp. d878 –d899.

Hyvärinen, Aapo (1999). „Fast and robust fixed-point algorithms for independent component analysis“. In: *IEEE transactions on neural networks* 10 3, pp. 626–34.

Jacomy, Mathieu, Tommaso Venturini, Sebastien Heymann, and Mathieu Bastian (2014). „ForceAtlas2, a continuous graph layout algorithm for handy network visualization designed for the Gephi software“. In: *PloS one* 9.6, e98679.

Jenkinson, Mark and Michael Chappell (2018). *Introduction to Neuroimaging Analysis*. Oxford Neuroimaging Primers. OUP Oxford.

Jenkinson, Mark and Stephen M. Smith (2001). „A global optimisation method for robust affine registration of brain images“. In: *Medical image analysis* 5 2, pp. 143–56.

Jenkinson, Mark, Peter R. Bannister, Michael A Brady, and Stephen Smith (2002). „Improved optimization for the robust and accurate linear registration and motion correction of brain images.“ In: *NeuroImage* 17 2, pp. 825–41.

Kobayashi, Masahito and Alvaro Pascual-Leone (2003). „Transcranial magnetic stimulation in neurology.“ In: *The Lancet. Neurology* 2 3, pp. 145–56.

Krüger, G. and G. H. Glover (2001). „Physiological noise in oxygenation-sensitive magnetic resonance imaging.“ In: *Magnetic resonance in medicine* 46 4, pp. 631–7.

Kuramoto, Yoshiki (1984). *Chemical oscillations, waves, and turbulence*. Vol. 19. Springer Science & Business Media.

Lancichinetti, Andrea and Santo Fortunato (2012). „Consensus clustering in complex networks“. In: *Scientific Reports*.

Leitao, J., A. Thielscher, J. Tunnerhoff, and U. Noppeney (2015). „Concurrent TMS-fMRI Reveals Interactions between Dorsal and Ventral Attentional Systems“. In: *Journal of Neuroscience*.

Logothetis, Nikos K. (2008). *What we can do and what we cannot do with fMRI*.

Logothetis, Nikos K., Mark Augath, Yusuke Murayama, et al. (2010). „The effects of electrical microstimulation on cortical signal propagation“. In: *Nature Neuroscience*.

Maccabee, P. J., V. E. Amassian, Roger Q Cracco, et al. (1991). „Magnetic coil stimulation of human visual cortex: studies of perception.“ In: *Electroencephalography and clinical neurophysiology. Supplement* 43, pp. 111–20.

Mastropasqua, Chiara, Marco Bozzali, Viviana Ponzo, et al. (2014). „Network based statistical analysis detects changes induced by continuous theta-burst stimulation on brain activity at rest“. In: *Frontiers in Psychiatry*.

Menon, V (2015). „Salience Network“. In: *Brain mapping: An encyclopedic reference*. Ed. by Arthur W Toga. Vol. 2. Academic Press, pp. 597–611.

Min, Yu-Sun, Jang Woo Park, Seong Uk Jin, et al. (2016). „Neuromodulatory effects of offline low-frequency repetitive transcranial magnetic stimulation of the motor cortex: A functional magnetic resonance imaging study“. In: *Scientific reports* 6, p. 36058.

Muldoon, Sarah Feldt, Fabio Pasqualetti, Shi Gu, et al. (2016). „Stimulation-based control of dynamic brain networks“. In:

Murphy, Kevin, Rasmus M. Birn, Daniel A. Handwerker, Tyler B. Jones, and Peter A. Bandettini (2009). „The impact of global signal regression on resting state correlations: Are anti-correlated networks introduced?“ In: *NeuroImage* 44 3, pp. 893–905.

Nelson, Steven M., Nico U. F. Dosenbach, Alexander L. Cohen, et al. (2010). „Role of the anterior insula in task-level control and focal attention“. In: *Brain Structure and Function*.

Nettekoven, C., L. J. Volz, M. Kutscha, et al. (2014). „Dose-Dependent Effects of Theta Burst rTMS on Cortical Excitability and Resting-State Connectivity of the Human Motor System“. In: *Journal of Neuroscience*.

O’Shea, Jacinta, Heidi Johansen-Berg, Danielle Trief, Silke Göbel, and Matthew F.S. Rushworth (2007). „Functionally Specific Reorganization in Human Premotor Cortex“. In: *Neuron*.

Pascual-Leone, Alvero, Josep Valls-Solé, Esther Wassermann, and Maurice Hallett (1994). „Responses to rapid-rate transcranial magnetic stimulation of the human motor cortex.“ In: *Brain : a journal of neurology* 117 (Pt 4), pp. 847–58.

Polania, Rafael, Michael A. Nitsche, and Christian C. Ruff (2018). *Studying and modifying brain function with non-invasive brain stimulation*.

Power, Jonathan D., Alexander L. Cohen, Steven M. Nelson, et al. (2011). „Functional Network Organization of the Human Brain". In: *Neuron* 72.4, pp. 665–678.

Power, Jonathan D., Anish Mitra, Timothy O. Laumann, et al. (2014). „Methods to detect, characterize, and remove motion artifact in resting state fMRI". In: *NeuroImage* 84, pp. 320–41.

Preibisch, Christine, Ulrich Pilatus, Juergen Bunke, et al. (2003). „Functional MRI using sensitivity-encoded echo planar imaging (SENSE-EPI)." In: *NeuroImage* 19 2 Pt 1, pp. 412–21.

Preibisch, Christine, Gabriel Castrillon, Martin Bührer, and Valentin Riedl (2015). „Evaluation of multiband EPI acquisitions for resting state fMRI". In: *PloS one* 10.9, e0136961.

Pruessmann, Klaas P., Michael C. Weiger, Madleina Scheidegger, and Peter Boesiger (1999). „SENSE: sensitivity encoding for fast MRI." In: *Magnetic resonance in medicine* 42 5, pp. 952–62.

Rahnev, D., P. Kok, M. Munneke, et al. (2013). „Continuous theta burst transcranial magnetic stimulation reduces resting state connectivity between visual areas". In: *Journal of Neurophysiology*.

Reithler, J., J. C. Peters, and A. T. Sack (2011). *Multimodal transcranial magnetic stimulation: Using concurrent neuroimaging to reveal the neural network dynamics of noninvasive brain stimulation*.

Rossini, P. M., Deborah S. D. Burke, Royce W. S. Chen, et al. (2015). „Non-invasive electrical and magnetic stimulation of the brain, spinal cord, roots and peripheral nerves: Basic principles and procedures for routine clinical and research application. An updated report from an I.F.C.N. Committee". In: *Clinical Neurophysiology* 126, pp. 1071–1107.

Rubinov, Mikail (2015). „Neural networks in the future of neuroscience research". In: *Nature Reviews Neuroscience* 16, pp. 767–767.

Rubinov, Mikail and Olaf Sporns (2010). „Complex network measures of brain connectivity: Uses and interpretations". In: *NeuroImage* 52 3, pp. 1059–69.

– (2011). „Weight conserving characterization of complex functional brain networks". In: *Neuroimage* 56.4, pp. 2068–2079.

Ruff, Christian C., Felix Blankenburg, Otto Bjoertomt, et al. (2006). „Concurrent TMS-fMRI and Psychophysics Reveal Frontal Influences on Human Retinotopic Visual Cortex". In: *Current Biology*.

Schindler, Kaspar, Thomas Nyffeler, Roland Wiest, et al. (2008). „Theta burst transcranial magnetic stimulation is associated with increased EEG synchronization in the stimulated relative to unstimulated cerebral hemisphere." In: *Neuroscience letters* 436 1, pp. 31–4.

Setsompop, Kawin, Borjan Gagoski, Jonathan R. Polimeni, et al. (2012). „Blipped-controlled aliasing in parallel imaging for simultaneous multislice echo planar imaging with reduced g-factor penalty." In: *Magnetic resonance in medicine* 67 5, pp. 1210–24.

Silvanto, Juha, Neil G. Muggleton, Alan Cowey, and Vincent Walsh (2007). „Neural activation state determines behavioral susceptibility to modified theta burst transcranial magnetic stimulation." In: *The European journal of neuroscience* 26 2, pp. 523–8.

Smith, Stephen M (2002). „Fast robust automated brain extraction.“ In: *Human brain mapping* 17 3, pp. 143–55.

Sollmann, Nico, Noriko Tanigawa, Lucia Bulubas, et al. (2016). „Clinical Factors Underlying the Inter-individual Variability of the Resting Motor Threshold in Navigated Transcranial Magnetic Stimulation Motor Mapping“. In: *Brain Topography* 30, pp. 98–121.

Spadone, Sara, Stefania Della Penna, Carlo Sestieri, et al. (2015). „Dynamic reorganization of human resting-state networks during visuospatial attention.“ In: *Proceedings of the National Academy of Sciences of the United States of America* 112 26, pp. 8112–7.

Sporns, Olaf and Richard F Betzel (2016). „Modular brain networks“. In: *Annual review of psychology* 67, pp. 613–640.

Thut, Gregor and Alvaro Pascual-Leone (2009). „A Review of Combined TMS-EEG Studies to Characterize Lasting Effects of Repetitive TMS and Assess Their Usefulness in Cognitive and Clinical Neuroscience“. In: *Brain Topography* 22, pp. 219–232.

Tik, Martin, André Hoffmann, Ronald Sladky, et al. (2017). „Towards understanding rTMS mechanism of action: Stimulation of the DLPFC causes network-specific increase in functional connectivity“. In: *NeuroImage*.

Triantafyllou, Christina, Rick Hoge, G. Krüger, et al. (2005). „Comparison of physiological noise at 1.5 T, 3 T and 7 T and optimization of fMRI acquisition parameters.“ In: *NeuroImage* 26 1, pp. 243–50.

Triantafyllou, Christina, Richard D. Hoge, and Lawrence L. Wald (2006). „Effect of spatial smoothing on physiological noise in high-resolution fMRI.“ In: *NeuroImage* 32 2, pp. 551–7.

Triantafyllou, Christina, Jonathan R. Polimeni, and Lawrence L. Wald (2011). „Physiological noise and signal-to-noise ratio in fMRI with multi-channel array coils“. In: *NeuroImage* 55 2, pp. 597–606.

Uddin, Lucina Q. (2015). „Salience processing and insular cortical function and dysfunction“. In: *Nature Reviews Neuroscience* 16, pp. 55–61.

Valchev, Nikola, Branislava Curčić-Blake, Remco J. Renken, et al. (2015). „cTBS delivered to the left somatosensory cortex changes its functional connectivity during rest“. In: *NeuroImage*.

Valero-Cabré, Antoni, Julià L. Amengual, Chloé Stengel, Alvaro Pascual-Leone, and Olivier A. Coubard (2017). *Transcranial magnetic stimulation in basic and clinical neuroscience: A comprehensive review of fundamental principles and novel insights*.

Van Den Heuvel, Martijn, Rene Mandl, and Hilleke Hulshoff Pol (2008). „Normalized cut group clustering of resting-state FMRI data“. In: *PloS one* 3.4, e2001.

Ven, Vincent van de and Alexander T. Sack (2013). „Transcranial magnetic stimulation of visual cortex in memory: Cortical state, interference and reactivation of visual content in memory“. In: *Behavioural Brain Research* 236, pp. 67–77.

Wang, Jane X., Lynn M. Rogers, Evan Z. Gross, et al. (2014). „Memory Enhancement: Targeted enhancement of cortical-hippocampal brain networks and associative memory“. In: *Science*.

Watanabe, T., R. Hanajima, Y. Shirota, et al. (2015). „Effects of rTMS of Pre-Supplementary Motor Area on Fronto Basal Ganglia Network Activity during Stop-Signal Task“. In: *Journal of Neuroscience*.

Watanabe, Takamitsu, Ritsuko Hanajima, Yuichiro Shirota, et al. (2014). „Bidirectional effects on interhemispheric resting-state functional connectivity induced by excitatory and inhibitory repetitive transcranial magnetic stimulation“. In: *Human Brain Mapping*.

Werf, Ysbrand D. van der and Tomás Paus (2006). „The neural response to transcranial magnetic stimulation of the human motor cortex. I. Intracortical and cortico-cortical contributions“. In: *Experimental Brain Research* 175, pp. 231–245.

Werf, Ysbrand D. van der, Ernesto J. Sanz-Arigita, Sanne Menning, and Odile A. van den Heuvel (2010). „Modulating spontaneous brain activity using repetitive transcranial magnetic stimulation“. In: *BMC Neuroscience*.

Winkler, Anderson M., Gerard R. Ridgway, Matthew A. Webster, Stephen M. Smith, and Thomas E. Nichols (2014). „Permutation inference for the general linear model“. In: *NeuroImage*.

Xu, Junqian, Steen Moeller, Edward J. Auerbach, et al. (2013). „Evaluation of slice accelerations using multiband echo planar imaging at 3 T“. In: *NeuroImage* 83, pp. 991–1001.

Yeo, BTT, Fenna M Krienen, Jorge Sepulcre, et al. (2011). „The organization of the human cerebral cortex estimated by intrinsic functional connectivity“. In: *Journal of neurophysiology* 106.3, pp. 1125–1165.

Yeo, BTT, Fenna M. Krienen, Michael W. L. Chee, and Randy L. Buckner (2014). „Estimates of segregation and overlap of functional connectivity networks in the human cerebral cortex“. In: *NeuroImage* 88, pp. 212–27.

Zang, Yu-Feng, Yong He, Chao-Zhe Zhu, et al. (2007). „Altered baseline brain activity in children with ADHD revealed by resting-state functional MRI.“ In: *Brain & development* 29 2, pp. 83–91.

Zang, Yufeng, Tianzi Jiang, Yingli Lu, Yong He, and Lixia Tian (2004). „Regional homogeneity approach to fMRI data analysis.“ In: *NeuroImage* 22 1, pp. 394–400.

Zou, Qi-Hong, Chao-Zhe Zhu, Yihong Yang, et al. (2008). „An improved approach to detection of amplitude of low-frequency fluctuation (ALFF) for resting-state fMRI: fractional ALFF.“ In: *Journal of neuroscience methods* 172 1, pp. 137–41.

Web references

CPAC. *CPAC website*. URL: `http://fcp-indi.github.io/docs/user/sca.html`.

OHBA. *OHBA-Oxford*. URL: `https://www.ohba.ox.ac.uk/facilities/copy_of_transcranial-magnetic-stimulation-tms`.

List of Figures

List of Tables

Acronyms

AIC anterior insular cortex.

ALFF amplitude of low frequency fluctuations.

aMT active motor threshold.

BOLD blood-oxygen-level-dependent.

CEN central executive network.

cTBS continuous TBS.

dACC dorsal anterior cingulate cortex.

DAN dorsal attention network.

DAPFC dorsoanterior prefrontal cortex.

DLPFC dorsolateral prefrontal cortex.

DMN default mode network.

EEG electroencephalography.

EPI echo planar imaging.

fALFF fractional ALFF.

FC functional connectivity.

FEF frontal eye fields.

fMRI functional magnetic resonance imaging.

g geometric factor.

GM gray matter.

ICA independent component analysis.

iFC intrinsic functionally connected.

IPL inferior parietal lobule.

IPS intraparietal sulcus.

iTBS intermittent TBS.

M1 primary motor cortex.

mb multiband.

MEG magnetoencephalography.

MEP motor evoked potential.

MFG middle frontal gyrus.

MRI magnetic resonance imaging.

MTG middle temporal gyrus.

NIBS Non-invasive brain stimulation.

PCG posterior cingulate gyrus.

PCUN precuneus.

PET positron emission tomography.

PMd dorsal premotor cortex.

pre-SMA pre-supplementary motor area.

ReHo regional homogeneity.

RF radio-frequency.

rMT resting motor threshold.

rs-fMRI resting state fMRI.

rTMS repetitive TMS.

S1 primary somatosensory cortex.

SAL salience network.

SCA seed-based correlation analysis.

SM sensory-motor network.

SPL superior parietal lobule.

TBS theta-burst stimulation.

tES transcranial electrical stimulation.

TMS transcranial magnetic stimulation.

TR repetition time.

tSNR temporal signal to noise ratio.

VIS visual network.

WM white matter.

Publications related to thesis

Scientific articles

1. Preibisch, Christine & **Gabriel Castrillon**, Martin Bührer and Valentin Riedl (2015). „Evaluation of multiband EPI acquisitions for resting state fMRI“. In: PloS one 10.9, e0136961

2. **Gabriel Castrillon**, Nico Sollmann, Katarzyna Kurcyus, Sandro Krieg and Valentin Riedl (2018). „Brain functional integration indicates spreadig effects of TMS“. In preparation for publication

Awards

1. Abstract Merit Award Organization for Human Brain Mapping (OHBM) 2018

Oral presentations

1. „Inhibitory TMS differentially affects brain network communication depending on the stimulation site“. Annual meeting Organization for Human Brain Mapping (OHBM) 2018

2. „Inhibitory TMS differentially affects brain network communication depending on the stimulation site“. Annual Brain Stimulation and Imaging Meeting (Brainstim) 2018

3. „Brain functional integration indicates cortical spreading of brain stimulation effect“. Symposium of the TUM-Neuroimaging center (TUM-NIC) 2018

Poster presentations

1. „Inhibitory TMS differentially affects brain network communication depending on the stimulation site“. Annual meeting Organization for Human Brain Mapping (OHBM) 2018

2. „Inhibitory TMS differentially affects brain network communication depending on the stimulation site“. Annual Brain Stimulation and Imaging Meeting (Brainstim) 2018

3. „Testing and disturbing communication in functional brain networks using TMS“. Annual meeting Organization for Human Brain Mapping (OHBM) 2016

4. „Testing and disturbing communication in functional brain networks using TMS“. Annual Brain Stimulation and Imaging Meeting (Brainstim) 2016

Colophon

This thesis was typeset with LaTeX 2_ε. It uses the *Clean Thesis* style developed by Ricardo Langner. The design of the *Clean Thesis* style is inspired by user guide documents from Apple Inc.

Download the *Clean Thesis* style at `http://cleanthesis.der-ric.de/`.